Preparation of Organometallic Ruthenium–Arene–Diaminotriazine Complexes as Binding Agents to DNA

ARTICLE *in* CHEMISTRY - AN ASIAN JOURNAL · APRIL 2012

Impact Factor: 4.59 · DOI: 10.1002/asia.201100883 · Source: PubMed

CHEMISTRY
AN ASIAN JOURNAL

DOI: 10.1002/asia.201100883

Preparation of Organometallic Ruthenium–Arene–Diaminotriazine Complexes as Binding Agents to DNA

Natalia Busto,[a] Jesús Valladolid,[a] Cristina Aliende,[a] Félix A. Jalón,[b] Blanca R. Manzano,[b] Ana M. Rodríguez,[b] Jorge F. Gaspar,[c] Celia Martins,[c] Tarita Biver,[d] Gustavo Espino,*[a] José María Leal,[a] and Begoña García*[a]

Abstract: The reactions of two diaminotriazine ligands 2,4-diamino-6-(2-pyridyl)-1,3,5-triazine (2-pydaT) and 6-phenyl-2,4-diamino-1,3,5-triazine (PhdaT) with ruthenium–arene precursors led to a new family of ruthenium(II) compounds that were spectroscopically characterized. Four of the complexes were cationic, with the general formula [(η^6-arene)Ru(κ^2-*N*,*N*-2-pydaT)Cl]X (X = BF_4, TsO; arene = *p*-cymene: **1**·BF_4, **1**·TsO; arene = benzene: **2**·BF_4, **2**·TsO). The neutral cyclometalated complex [(η^6-*p*-cymene)Ru(κ^2-*C*,*N*-PhdaT*)Cl] (**3**) was also isolated. The structures of complexes **2**·BF_4 and **3**·H_2O were determined by X-ray diffraction. Complex **1**·BF_4 underwent a partial reversible-aquation process in water. UV/Vis and NMR spectroscopic measurements showed that the reaction was hindered by the addition of NaCl and was pH-controlled in acidic solution. At pH 7.0 (sodium cacodylate) Ru–Cl complex **1**·BF_4 was the only species present in solution, even at low ionic strength. However, in alkaline medium (KOH), complex **1**·BF_4 underwent basic hydrolysis to afford a Ru–OH complex (**5**). Fluorimetric studies revealed that the interaction of complex **1**·BF_4 with DNA was not straightforward; instead, its main features were closely linked to ionic strength and to the [DNA]/complex ratio. The bifunctional complex **1**·BF_4 was capable of interacting concurrently through both its *p*-cymene and 2-pydaT groups. Cytotoxicity and genotoxicity studies showed that, contrary to the expected behavior, the complex species was biologically inactive; the formation of a Ru–OH complex could be responsible for such behavior.

Keywords: arenes · DNA · organometallic complexes · ruthenium · triazines

Introduction

The breakthrough synthesis of cisplatin in 1965 revolutionized cancer chemotherapy and opened new horizons in the search for new metal-based drugs.[1–3] Decades later, it is still one of the most-efficient treatments in clinical use despite its side-effects.[4] Since then, a lot of metallic compounds have been investigated, and a few of them have been successfully used as anticancer drugs. Moreover, we have learnt that both the pharmacological targets and the modes of action are not universal. Consequently, open-minded strategies must be conceived not only in the design but also in the evaluation of these metallodrugs.

More recently, organometallic compounds have emerged as a very interesting alternative resource in medicinal chemistry for several reasons. First of all, these hybrids combine features of both, the metallic center and one or more organic fragments. On the one hand, these compounds are endowed with the versatile stereochemistry and redox properties of the corresponding metal cation, together with its ability to bind to biological targets. On the other hand, organometallic species can exhibit a huge variety of functionalized organic ligands with very specific reactivities. In particular, it is possible to prepare sturdy Ru^{II}–arene complexes of the general formula [(η^6-arene)$RuCl_2$(L)] or [(η^6-arene)RuCl(L-L)]Y, where the characteristic π-bonded arene is relatively inert to displacement under physiological conditions[4] and provides redox stability by withdrawing electronic density from the metal ion.[5] These arenes may

[a] Dr. N. Busto, J. Valladolid, C. Aliende, Dr. G. Espino, Prof. J. M. Leal, Prof. B. García
Departamento de Química
Facultad de Ciencias. Universidad de Burgos
Plaza Misael Bañuelos s.n., 09001, Burgos (Spain)
Fax: (+34) 947-258831
E-mail: gespino@ubu.es
begar@ubu.es

[b] Prof. F. A. Jalón, Prof. B. R. Manzano, Dr. A. M. Rodríguez
Departamento de Química Inorgánica, Orgánica y Bioquímica
Facultad de Químicas-IRICA. Universidad de Castilla-La Mancha
Avda. Camilo José Cela, 10, 13071, Ciudad Real (Spain)

[c] Prof. J. F. Gaspar, C. Martins
Departamento de Genética
Universidade Nova de Lisboa
Faculdade de Ciencias Médicas, CIGMH
1349-008, Lisboa (Portugal)

[d] Dr. T. Biver
Chemistry and Industrial Chemistry Department
University of Pisa
56126 Pisa (Italy)

Supporting information for this article is available on the WWW under http://dx.doi.org/10.1002/asia.201100883.

also enhance transport ability through cellular membranes and modulate the reactivity and cytotoxicity of the complexes.[6] In any case, the introduction of hydrophilic groups onto any of the ligands confers solubility in aqueous physiological media. Thus, Ru^{II}–arene complexes are among the most-promising candidates for entering clinical trials, and the research groups of Sadler and Dyson are pioneering this research. Sadler and co-workers have developed a family of drugs of the formula $[(\eta^6\text{-arene})RuCl(en)]PF_6$ that are cytotoxic to cancer cells, including cis-platin-resistant cell lines,[7,8] and whose biological target is thought to be DNA.[9,10] On the other hand, Dyson and co-workers have focused on the RAPTA family; these Ru^{II}–arene compounds contain the hydrophilic and monodentate 1,3,5-triaza-7-phosphatricyclo-[3.3.1.1]decane (pta) ligand, and some members of the group, such as $[(\eta^6\text{-toluene})RuCl_2(pta)]$, show selectivity towards metastatic tumors.[11] Many other research groups are also contributing to increase the number of potential ruthenium anticancer drugs as well, and some recent reviews have given detailed perspectives on this subject.[11–16]

2,4-Diamino-1,3,5-triazine derivatives own a well-known biological activity, and some of them have been described as potential chemotherapeutic agents for leukaemia, melanoma, and breast cancer because of their antiproliferative activities.[17–19] They interact with DNA by intercalating into the base-pairs of the polynucleotide.[20] Moreover, some examples of metal complexes with different triazine hybrids have been reported that exhibit good activity in the inhibition of cancer-cell growth.[21,22] However, to the best of our knowledge, complexes of 2,4-diamino-1,3,5-triazines have not yet been explored in this field.

For its part, the Cl substituents on Pt- and Ru prodrugs are kinetically labile and can undergo aquation or hydroxylation processes to give either aqua- or hydroxo complexes;[23] the former are even more labile than their corresponding chloro complexes and are regarded as the active forms of the drugs, whereas the hydroxo species are less prone to substitution reactions and are thought to be inactive derivatives.[6,23–25] This feature holds a great deal of promise because the extracellular chloride content is higher than the intracellular one. Therefore, aquation takes place inside the cell, which usually favors the reaction with DNA in a similar way as occurs with cisplatin.[2,3] However, because the octahedral structure of the Ru^{II} complexes is different from the square-planar geometry of Pt^{II} species, the interaction with DNA presumably occurs in a different manner from that of cisplatin. As a matter of fact, DNA is one of the most common anticancer biological targets, though by no means the only one, and many metal complexes have been designed to bind selectively to specific sequences of nucleic acids. In particular, some anticancer Ru^{III} compounds, currently in clinical trials, are reduced in hypoxic tumoral areas to their active Ru^{II} forms, which bind to cellular DNA.[26,27] Moreover, the majority of Ru^{II}–arene complexes may interact with guanine residues, thereby forming monofunctional adducts, whilst some also interact noncovalently with DNA through the arene moiety, mainly by external binding.[7,28,29] Other biological targets have also been reported for anticancer arene–ruthenium complexes. For instance, RAPTA compounds behave as inhibitors of the proteins cathepsin B and thioredoxin reductase.[30] On the other hand, complexes of the formula $[(\eta^6\text{-arene})Ru(azpy)I]^+$ (azpy = *N*,*N*-dimethylphenyl or hydroxyphenylazopyridine) catalytically oxidize glutathione into glutathione disulfide, thereby leading to an accumulation of reactive oxygen species (ROS), which explains the potent cytotoxic effect toward cancer cells.[31]

We assume that a combination of *p*-cymene, 2,4-diamino-1,3,5-triazine, and Cl ligands in the coordination sphere of a Ru^{II} ion could render the resulting complexes as excellent candidates as antitumor agents. Therefore, herein, we report the synthesis and characterization of a new family of Ru^{II}–arene complexes of 6-substituted-2,4-diamino-1,3,5-triazines and their in vitro anticancer performance. Moreover, we address the interaction of complex $[(\eta^6\text{-arene})RuCl(\kappa^2\text{-}N,N\text{-}2\text{-pydaT})]BF_4$ (2-pydaT = 2,4-diamino-6-(2-pyridyl)-1,3,5-triazine) into DNA and report two types of binding. These results indicate that the likely formation of a hydroxo derivative in the culture medium could be responsible for the lack of biological activity.

Results and Discussion

Synthesis and Structural Characterization

Cationic Complexes

Complexes of the general formula $[(\eta^6\text{-arene})RuCl(\kappa^2\text{-}N,N\text{-}2\text{-pydaT})]X$ (**1**·BF_4, **1**·TsO, **2**·BF_4, and **2**·TsO; Scheme 1), were obtained as racemic mixtures in one-pot processes by reacting the appropriate arene starting material with the chelating ligand 2-pydaT and the corresponding silver salt. The dimer $[\{(\eta^6\text{-}p\text{-cymene})Ru(\mu\text{-}Cl)Cl\}_2]$[32,33] was used to isolate complexes **1**·BF_4 and **1**·TsO [Scheme 2, Eq. (1)], whereas the monomer $[(\eta^6\text{-benzene})RuCl_2(CH_3CN)]$[34] was used to prepare complexes **2**·BF_4 and **2**·TsO [Scheme 2, Eq. (2)]. Standard work-up afforded the four complexes in good yields. Complexes with TsO^- anions were more soluble than their corresponding BF_4^- analogues in certain solvents.

Neutral Complex

The cycloruthenated complex $[Ru(\eta^6\text{-}p\text{-cymene})Cl(\kappa^2\text{-}C,N\text{-PhdaT*})]$ (**3**; Scheme 1) was prepared by treating a solution of $[\{(\eta^6\text{-}p\text{-cymene})Ru(\mu\text{-}Cl)Cl\}_2]$ in MeOH with PhdaT, in the presence of excess NEt_3 (1:2:2.5 molar ratio) at room temperature [Scheme 2, Eq. (3)]. The experimental conditions were optimized carefully to obtain this compound as the main product. However, a second minor cycloruthenated product was observed in solution, presumably as a consequence of aquation (see below).

These compounds were fully characterized by ^1H, ^{19}F (for BF_4^- salts), and $^{13}C\{^1H\}$ NMR spectroscopy, and also by IR spectroscopy, FAB mass spectrometry, molar conductivity,

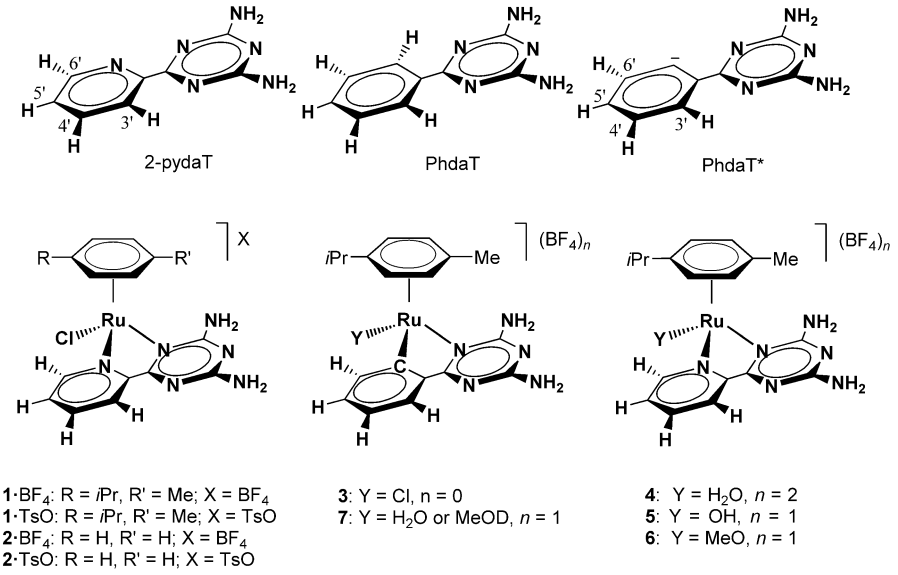

Scheme 1. Structures and numbering of ligands 2-pydaT, PhdaT, and PhdaT*, and Ru^{II}–arene complexes **1**–**7**. Complexes **4**–**7** were not isolated.

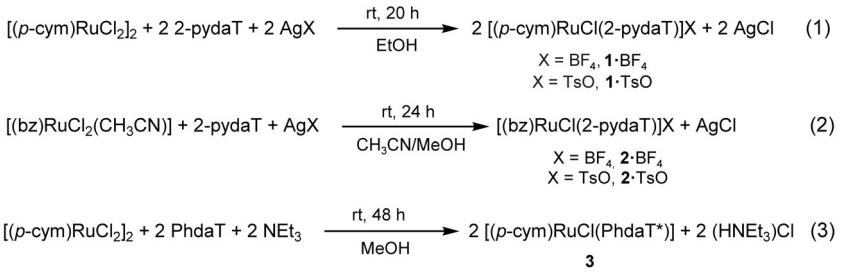

Scheme 2. Synthesis of complexes **1**·BF_4, **1**·TsO, **2**·BF_4, **2**·TsO, and **3**.

and elemental analysis. The structures of complexes **2**·BF_4 and **3** were determined by X-ray diffraction.

The ^{1}H NMR spectra of complexes **1**·BF_4, **1**·TsO, **2**·BF_4, and **2**·TsO showed the expected four multiplets for the pyridyl protons, the corresponding chemical shifts of which were almost all identical (see the Supporting Information, Table 1). Therefore, no counteranion- or arene effects were detected in the NMR resonances in CD_3OD. In all of these cases, these peaks appeared at higher frequencies than those of the free compound 2-pydaT, owing to complexation. This effect was especially apparent for the $H^{6'}$ proton, which was closest to the metal center (about 0.7 ppm downfield). The ^{1}H NMR spectrum of complex **3** also showed four signals for the phenyltriazine ring, thereby suggesting that C–H bond activation had occurred in PhdaT to produce a cycloruthenated species with a κ^2-*C*,*N* chelate ring. The *p*-cymene resonances of **1**·BF_4, **1**·TsO, and **3** revealed the stereogenic and chirotopic nature of the metal center (local C_1 symmetry).[35] Indeed, an ABCD spin system was observed for the aromatic protons and diastereotopic methyl groups were observed for the isopropyl moiety (see the Supporting Information, Table 2). This observation was in agreement with a bidentate coordination mode for the nitrogenated ligands. Signals corresponding to the NH_2 groups were not detected in CD_3OD, owing to rapid intermolecular H/D exchange with deuterium from the solvent. Thus, the ^{1}H NMR spectrum of complex **1**·BF_4 was also recorded in dry [D_6]DMSO (a strong hydrogen-bond acceptor) to avoid such exchange processes. Two broad resonances that were assignable to the NH_2 groups were observed at $\delta =$ 8.42 and 6.28 ppm, which indicated that the two amine groups were inequivalent, and was additional evidence for coordination. The resonances of the corresponding anions were observed in compounds **1**·TsO and **2**·TsO.

All of the resonances for compound **3** were more shielded than those for cation **1**. In particular, the higher field chemical shifts of the *p*-cymene resonances in compound **3** suggested higher back-bonding from the Ru ion to the ring, which could be a result of the greater donating ability of PhdaT* compared to 2-pydaT, owing to the formal anionic nature of PhdaT*.

Interestingly, the spectrum of compound **3** in wet CD_3OD showed a set of secondary signals that were assigned to the solvolysis product [Ru(η^6-*p*-cymene)(κ^2-*C*,*N*-PhdaT*)(S)]Cl (**7**; S = solvent, that is, water or CD_3OD; Scheme 1). These secondary signals were immediately suppressed on addition of excess NaCl to the NMR sample, thereby leaving compound **3** as the only product in solution.

Finally, the ^{1}H-NOESY spectra of complexes **1**·BF_4 and **1**·TsO suggested that certain orientations of the *p*-cymene ring and also of the *i*Pr group were preferred in solution. Selective NOE effects were observed between the H^8 and H^2 protons on one side of the ring, and between the H^9 and H^6 protons on the other side; this result was evidence for the restricted rotation of the *i*Pr group. In addition, a very intense NOE effect was detected between the resonance of the spatial reporter proton ($H^{6'}$) and those of the isochronous $H^{5,6}$ protons, whereas NOE interactions between the $H^{6'}$and H^2 protons and between the $H^{6'}$ and H^3 protons showed decreasing intensities ($H^{5,6} > H^2 > H^3$; see Scheme 1, also see the Supporting Information). This result suggested that certain orientations for the *p*-cymene group were pre-

CHEMISTRY
AN ASIAN JOURNAL

ferred because of steric hindrance. Thus, conformations A and B (Scheme 3), and to a lesser degree E and D, were favored to the detriment of C and F. Zuccaccia and Macchioni reported a similar conformational study.[36]

The $^{13}C\{^1H\}$ NMR spectra of complexes **1·BF$_4$**, **1·TsO**, **2·BF$_4$**, and **2·TsO** in CD_3OD showed almost identical signals for the carbon atoms of the coordinated 2-pydaT group (see the Supporting Information, Table 3). For the *p*-cymene de-

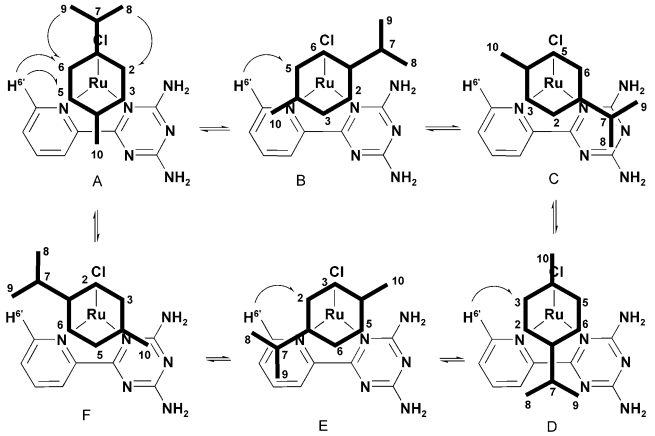

Scheme 3. Possible eclipsed conformations of *p*-cymene in complexes **1**·BF_4 and **1**·TsO, where A, B, D, and E are the most-favored rotamers, according to the observed NOE effects (see arrows).

rivatives, the data confirmed the C_1 local symmetry of the ring and the κ^2-*N*,*N* coordination mode for the nitrogenated ligand. We could not record a high quality $^{13}C\{^1H\}$ NMR spectrum of compound **3** because of its low solubility.

In the FAB mass spectra, all of the ionic complexes (**1**·BF_4, **1**·TsO, **2**·BF_4, and **2**·TsO) showed peaks corresponding to their respective parent cationic species, $[M-BF_4]^+$ or $[M-TsO]^+$, and also for species corresponding to the loss of the Cl^- ion and of the arene.

The IR spectra of all of the complexes showed several characteristic IR bands for the diaminotriazine ligands at $>3300\ cm^{-1}$(NH_2) and in the range of 1400–1650 cm^{-1} (C=C and C=N). In particular, the band at around 1514 cm^{-1} appeared shifted to lower energy with respect to that of the free ligand (at 1541 cm^{-1}), thereby suggesting N-coordination. Furthermore, the bands expected for the BF_4^- or TsO^- anions were also observed.

Molar conductivity measurements were carried out in CH_3CN at room temperature for all of the cationic compounds, thereby confirming the expected (1:1) ion electrolyte type. Complexes with TsO^- counterions showed lower Λ_M values compared to the corresponding complexes with BF_4^- counterions (see the Experimental Section).

Crystal Structures of Compounds 2·BF$_4$ and 3·H$_2$O

The molecular and crystalline structures of compounds **2**·BF_4 and **3** monohydrate (**3**·H_2O) were determined by single-crystal X-ray diffraction (Figure 1). Selected bond lengths and angles are given in Table 1, and relevant crystallographic parameters are listed in the Supporting Information, Table 4.

Both complexes crystallized in the monoclinic space group *P*21/*c* as mixtures of two enantiomers (R_{Ru} and S_{Ru}), owing to the chirality on the metal atoms. In the two molecular structures, the classical three-legged piano-stool arrangement was observed with a pseudo-octahedral geometry of the metal center. The coordination sphere of the Ru^{II} ion

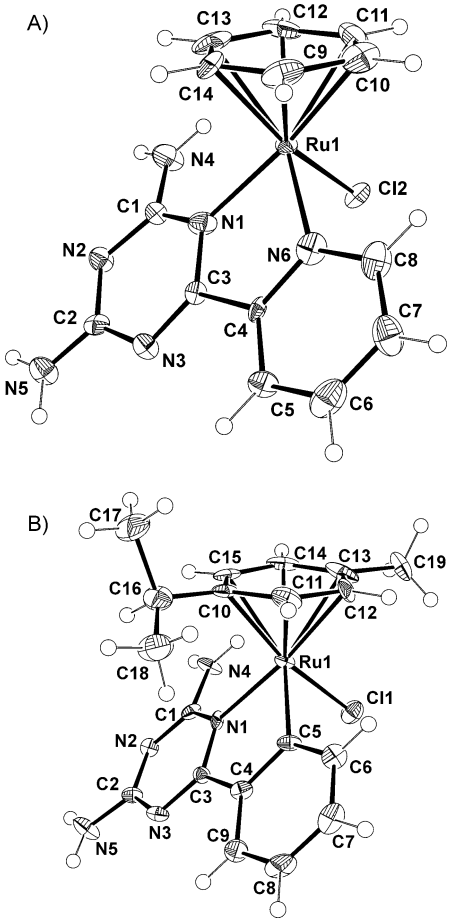

Figure 1. ORTEP of the *S* enantiomers of A) **2**·BF_4 and B) **3**·H_2O. The counteranion has been omitted from **2**·BF_4.

Table 1. Selected bond lengths [Å] and angles [°] for [(η^6-bz)RuCl(2-pydaT)]BF_4 (**2**·BF_4) and [(η^6-*p*-cym)RuCl(PhdaT*)] (**3**·H_2O).

Bond length/angle	**2**·BF_4	Bond length/angle	**3**·H_2O
Ru–arene (centroid)[a]	1.673	Ru–arene (centroid)[a]	1.711
Ru1–Cl2	2.393(3)	Ru1–Cl1	2.431(2)
Ru1–N1	2.100(9)	Ru1–N1	2.097(5)
Ru1–N6	2.07(1)	Ru1–C5	2.068(7)
N4–C1	1.321(16)	N4–C1	1.336(9)
N5–C2	1.301(16)	N5–C2	1.349(9)
N6-Ru1-N1	76.0(4)	C5-Ru1-N1	76.3(2)
N6-Ru1-Cl2	88.8(3)	C5-Ru1-Cl1	88.9(2)
N1-Ru1-Cl2	84.2(3)	N1-Ru1-Cl1	83.7(2)

[a] Calculated with Mercury, version 2.4.6.

contained an η^6-arene ring that occupied three facial coordination positions, a bidentate ligand (κ^2-*N*,*N*-2-pydaT for complex **2**·BF_4 and κ^2-*C*,*N*-PhdaT* for complex **3**·H_2O), and a chloride anion. The average Ru–centroid distances were 1.673 Å for benzene in complex **2**·BF_4 and 1.711 Å for *p*-cymene in complex **3**·H_2O, although both complexes showed significant variations in the Ru–C_{arene} bond lengths. The triazine ligands formed essentially planar five-membered chelate rings. The bite angles of these chelates were 76.0(4)° and 76.3(2)°, respectively. The Ru–$N_{pyridine}$ bond length was shorter than the Ru–$N_{triazine}$ bond, thus indicating that the pyridine N donor atom is a stronger σ donor. The Ru–C σ-bond length in complex **3**·H_2O was in the usual range[37] and the Ru–$N_{triazine}$ bond was similar in length to that of complex **2**·BF_4. The triazine rings were not completely planar in either complex **2**·BF_4 or complex **3**·H_2O and the amine groups adopted trigonal planar geometries with short C–NH_2 distances that were consistent with intermediate bonding between single and double bonds. The Ru–Cl bond lengths were 2.393(3) Å and 2.431(2) Å for complexes **2**·BF_4 and **3**·H_2O, respectively. In both cases, all of the coordination distances fit well within the known range for similar complexes. The orientation of the *p*-cymene ring in complex **3**·H_2O may have been influenced by the formation of a weak intramolecular hydrogen bond between the methyl group and the chloride ligand (H19C–Cl1 3.04 Å). This situation was also found in other Ru–*p*-cymene derivatives.[38] The structure of complex **2**·BF_4 resembled those of other complexes with the formula [(η^6-arene)RuCl(κ^2-*N*,*N*-L)]X, where ligand L coordinated through heteroaromatic rings[39,40] and complex **3**·H_2O compared well to [(η^6-*p*-cym)-RuCl(κ^2-*C*,*N*-Phpy)].[37] Intermolecular contacts in the solid-state structures of compounds **2**·BF_4 and **3**·H_2O are discussed in the Supporting Information.

*Stability of Complex **1**·BF_4 in Aqueous Solution: Aquation–Anation Equilibrium and Basic Hydrolysis*

Compound **1**·BF_4 was moderately soluble in water and so its stability in aqueous solution was studied by UV/Vis spectrometry at various ionic strengths (*I*) with NaCl, both in the presence and absence of buffer (sodium cacodylate). Figure 2 shows two isosbestic points (280 and 340 nm) using water as the solvent. A plot of absorbance (290 nm) versus time yielded a single exponential curve (Figure 2, inset) from which a rate constant of $7.5(\pm0.2)\times10^{-4}\ s^{-1}$ was obtained. The rate of hydrolysis diminished upon addition of NaCl; for $I=0.01$ M, the rate of hydrolysis dropped to $2.0(\pm0.2)\times10^{-5}\ s^{-1}$, and even became negligible at $I=0.1$ M.

The ^{1}H NMR spectrum of complex **1**·BF_4 (18 mM) in D_2O at room temperature was also recorded. A second minor product (**4**), which had C_1 local symmetry, was observed after 15 minutes along with complex **1**·BF_4 in an approximate 79:21 ratio (according to NMR integration; Figure 3 A). The sample was monitored periodically but no further changes were observed, even after several days, thus suggesting that equilibrium had been quickly reached. Then, an excess of NaCl was added to the sample and a spectrum

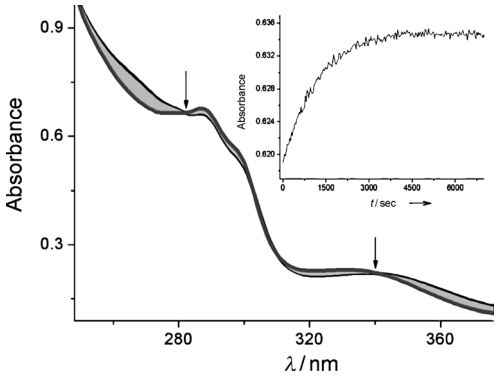

Figure 2. Variation of the absorbance spectra of **1**·BF_4 (0.18 mM) in water over 2 h; inset: kinetic monoexponential function at $\lambda=290$ nm.

was recorded again that only showed signals corresponding to the major product (**1**·BF_4; Figure 3 B). The minor product (**4**) was likely the result of aquation, and it was tentatively

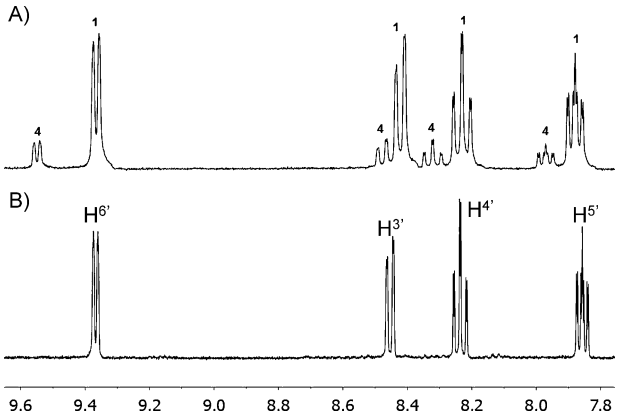

Figure 3. Aquation/anation equilibrium for **1**·BF_4. Low-field region of the ^{1}H NMR spectra of A) **1**·BF_4 in D_2O at 25 °C, which showed resonances corresponding to chloro-complex **1** (major) and aqua-complex **4** (minor) in a 79:21 ratio at equilibrium; and B) the same sample after adding an excess of NaCl, with labels for the **1**·BF_4 signals.

assigned as the dicationic aqua complex [(*p*-cym)Ru(OH_2)(2-pydaT)]$^{2+}$. We concluded that an aqueous solution of complex **1**·BF_4 gave rise to a rapid reversible aquation–anation equilibrium that was largely suppressed as the NaCl concentration was raised.[41] This behavior was in fairly good agreement with other cases where aquation transformed similar Ru–Cl complexes into their more-reactive aqua-derivatives, which have been proposed as the reactive intermediates for subsequent DNA interactions.[23]

In a second experiment, one equivalent of KOH was added to a solution of the equilibrated mixture of compounds **1**·BF_4 and **4** in D_2O (18 mM) and the sample was monitored at room temperature by ^{1}H NMR spectroscopy. Signals corresponding to the aqua-complex (**4**) were suppressed immediately, and peaks from a new product (**5**) were observed. After 2 hours, no signals corresponding to complex **1**·BF_4 remained and only those corresponding to

compound **5** were observed (Figure 4). This new derivative retained the *p*-cymene and triazine ligands and showed a similar C_1 pattern. Thus, we proposed that a new hydroxy species of the formula [(*p*-cym)Ru(OH)(2-pydaT)]BF_4 (**5**)

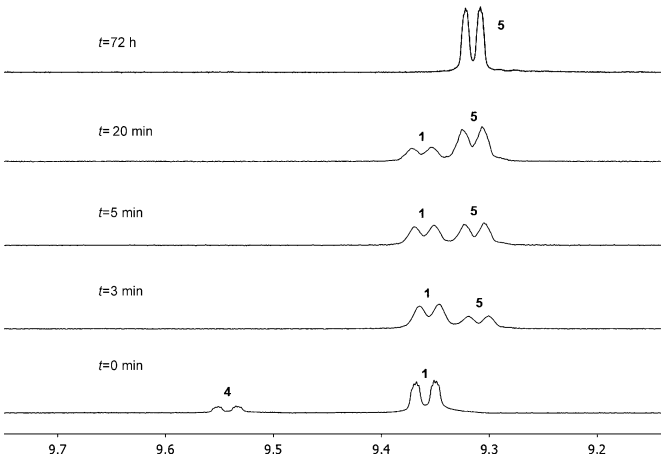

Figure 4. Change in the $H^{6'}$ resonance in the ^{1}H NMR spectrum of **1**·BF_4/KOH (1:1) in D_2O at 25 °C over time.

was formed at high pH values. Similar experiments (data not shown), which were performed in CD_3OD and in a mixture of CD_3OD/D_2O (1:4), afforded the methoxy complex [(*p*-cym)Ru(CD_3O)(2-pydaT)]BF_4 (**6**) in the first case, and a mixture of complexes **5** and **6** in the second. The formation of complex **6** was rationalized by taking into account that MeOH ($pK_a = 15.5$) is slightly more acidic than water ($pK_a = 15.7$). The spectra for the basic hydrolysis of complex **1**·BF_4 are shown in Figure 4 and the corresponding equilibria is given in Scheme 4. The synthesis of analogous Ru–OH derivatives have been reported from [Ru(η^6-arene)(en)(H_2O)]$^{2+}$[23] or from [Ru(η^6-*p*-cymene)Cl(H_2O)(pta)]$^{+}$[25] at alkaline pH.

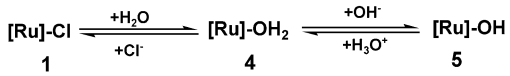

Scheme 4. Aquation/anation equilibrium and basic hydrolysis of compound **1**·BF_4. [Ru] = [(η^6-*p*-cymene)Ru(2-pydaT)]$(BF_4)_n$ ($n = 1$ for compounds **1** and **5**, $n = 2$ for compound **4**).

To properly assess the effect of pH, absorbance spectra were recorded as a function of time at low ionic strength ($I = 0.01$ M) and at various acidities (data not shown). The absorbance curves remained essentially unchanged, and no kinetic processes were observed. The acid-dissociation constants (pK_a) were determined potentiometrically at $I = 0.01$, 0.1, and 1.0 M (NaCl) by titration with NaOH (0.1 M). Owing to the presence of NaCl, hydrolysis processes could be neglected. The acidity constant remained unaffected by the change in ionic strength at $pK_a = 1.60$. On the basis of these results, we inferred that complex **1**·BF_4 remained unaffected at pH 7.0 (sodium cacodylate) and $I = 0.01$, 0.1, and 1.0 M (NaCl), which were the working conditions used to study the interaction with DNA (see below).

Binding of Ruthenium Complex 1·BF_4 to DNA

Binding Constants

The binding constants were evaluated by considering the fluorescence of ruthenium complex **1**·BF_4. The weak fluorescence observed in water was enhanced in the presence of NaCl, whilst it remained unchanged upon increasing the $NaClO_4$ content (see the Supporting Information, Figure 4). These results showed that it was specifically NaCl, rather than the ion strength, which was the main factor in the changes in fluorescence observed. The interaction between CT-DNA and **1**·BF_4 could be represented by:

$$D + P \rightleftharpoons DP \qquad (4)$$

where D and DP denote the free and bound **1**·BF_4, respectively, and P indicates the CT-DNA free sites. The equilibrium constant of [Eq. (4)] is:

$$K = \frac{[DP]}{[D] \times [P]} \qquad (5)$$

The binding constant of the apparent reaction [Eq. (4)] and the $\Delta\phi$ values were evaluated from the linear fitting of [Eq. (6)] to the relationship between $C_D/\Delta F$ and 1/[P]:

$$\frac{C_D}{\Delta F} = \frac{1}{\Delta\phi} + \frac{1}{K\Delta\phi} \times \frac{1}{[P]} \qquad (6)$$

where C_D is the total concentration of **1**·BF_4 and $\Delta F = F - \phi_D C_D$ represents the observed change in fluorescence (F) during the titration, $\phi_D = F^0/C_D$ (F^0 being the initial fluorescence of the **1**·BF_4 solution and $\Delta\phi = \phi_{PD} - \phi_D$ being the amplitude). The analysis required an iterative procedure. Initial data were introduced with $C_p = [P]$, C_P being the initial polymer concentration. The $\Delta\phi$ and K values obtained were reintroduced until convergence, which was attained after only three iterations.

Spectrofluorometric titrations were performed at $T = 25$ °C, pH 7.0, and at three different ionic strengths: 0.01, 0.1, and 1.0 M (NaCl; Figure 5). The binding isotherm displayed a biphasic behavior, and revealed the occurrence of two different modes of interaction: mode 1 and mode 2. Figure 5 A, which corresponded to the variation at $I = 0.01$, displayed a sharp decrease in the emission intensity upon the early addition of DNA to complex **1**·BF_4 (phase 1, see inset), followed by an increase in intensity (phase 2). The decrease in fluorescence emission observed for the first stretch of the titration curve persisted, even when the ionic strength was increased (Figure 5 B, C).

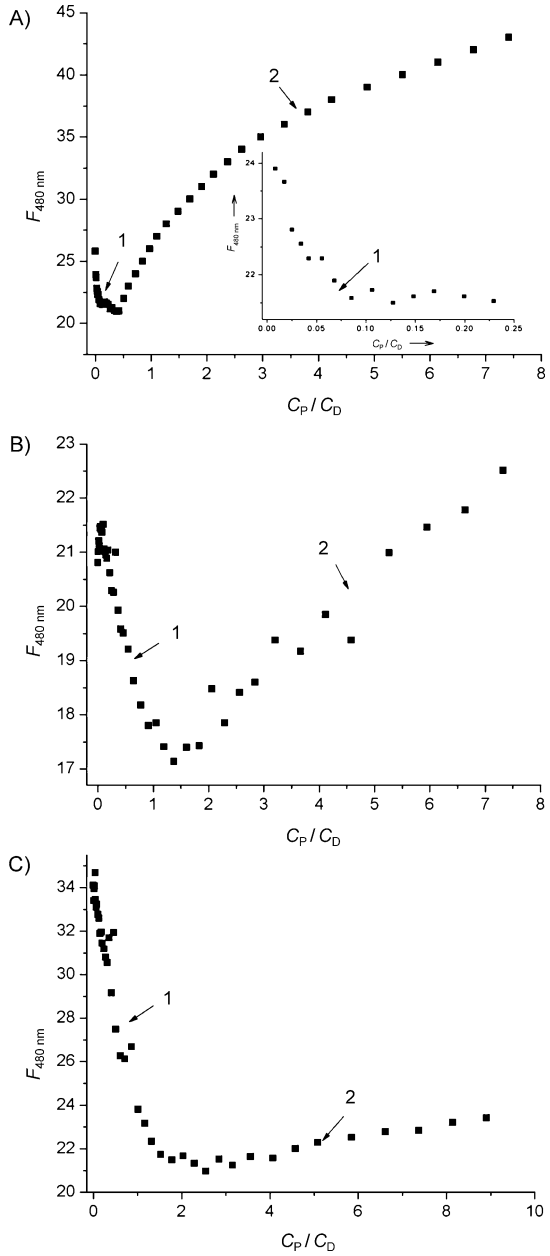

Figure 5. Fluorimetric binding isotherms of CT-DNA/**1**·BF_4 which show a biphasic behavior (modes of binding 1 and 2): $C^0_D = 1.0\times10^{-4}$ M, pH 7.0, and $T = 25$ °C. A) $I = 0.01$ M, B) $I = 0.1$ M, and C) $I = 1.0$ M.

Table 2. Fluorimetric equilibrium constants K_1 (corresponding to binding mode 1) and K_2 (binding mode 2) at different ionic strengths, pH 7.0, $T = 25$ °C.

I (NaCl) [M]	K_1 ($\times10^{-4}$) [M^{-1}]	K_2 ($\times10^{-3}$) [M^{-1}]
0.01	86.3(±13.2)	4.5(±0.2)
0.1	7.03(±0.77)	< 0.5
1.0	0.24(±0.10)	< 1.4

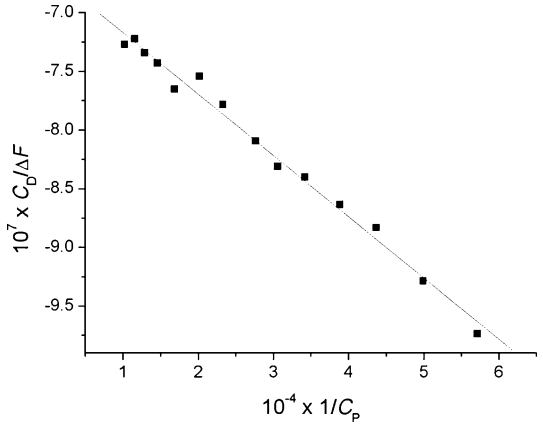

Figure 6. Fluorescence data from the first branch of the titration in Figure 5B fitted according to [Eq. (6)]; $C^0_D = 1.0\times10^{-4}$ M, pH 7.0, $I = 0.1$ M, $T = 25$ °C.

Binding Mode 1

Table 2 summarizes the K values at different ionic strengths, which corresponded to the analysis of phase 1 (binding mode 1) using [Eq. (6); Figure 6]. The equilibrium constants were of the same order of magnitude as those for the intercalation of proflavine into DNA ($K = 6.6\times10^4\,M^{-1}$, $I = 0.1$ M, $T = 25$ °C),[42] lower than those for the intercalation of [Ru(phen)$_2$(dppz)]$^{2+}$ (dppz = dipyrido[3,2-a:2′,3′-c]phenazine; $K = 1.3\times10^6\,M^{-1}$, $I = 0.012$ M, $T = 25$ °C)[43] and [Ru(dmb)$_2$(pdta)](ClO$_4$)$_2$ (dmb = 4,4′-dimethyl-2,2′-bipyridine, pdta = 3-(pyridine-2-yl)-as-triazino [5,6-f]-acenaphthylene; $K = 2.37\times10^5\,M^{-1}$),[44] higher than those for the surface interaction of [Ru(phen)$_2$dppz]$^{2+}$ (phen = 1,10-phenanthroline; $K = 2.3\times10^3\,M^{-1}$, $I = 0.012$ M, $T = 25$ °C),[43] and the same order of magnitude as those for the groove binding of pyridine-2-carbaldehyde thiosemicarbazonecopper(II) to [{poly(dA-dT)}$_2$] ($K = 4.56\times10^4\,M^{-1}$, $I = 0.1$ M).[45] These results were not conclusive enough on their own to discriminate in favor of the particular mode 1 of binding between ruthenium complex **1**·BF_4 and CT-DNA; the mode 1 of binding will be confirmed below as an external groove binding.

Binding Mode 2

The observed enhancement of the fluorescence emission in the second stretch of the titration occurred at low C_D content. This process was less evident at high ionic strengths, thereby revealing a strong electrostatic term of the Gibbs energy. Unfortunately, the binding constant of process 2 could not be evaluated accurately by using [Eq. 6] and only approximate values were obtained, except at $I = 0.01$ M. The low values of equilibrium constant K_2 of mode 2 were close to those found for pure electrostatic binding (ca. $100\,M^{-1}$ at $I = 0.11$ M and $1000\,M^{-1}$ at $I = 0.01$ M for ethidium/DNA[46] and $< 600\,M^{-1}$ at $I = 0.21$ M and $2.3\times10^3\,M^{-1}$ at $I = 0.012$ M[43] for [Ru(phen)$_2$dppz]$^{2+}$/DNA). The electrostatic external binding of mode 2 is confirmed below.

Concerning the salt effect on the mode 1 of binding, we found that an increase in the ionic strength of the medium caused a decrease in binding constant K (Table 2). Figure 7 shows a straight line plot of log K vs. $-\log[Na^+]$ that was

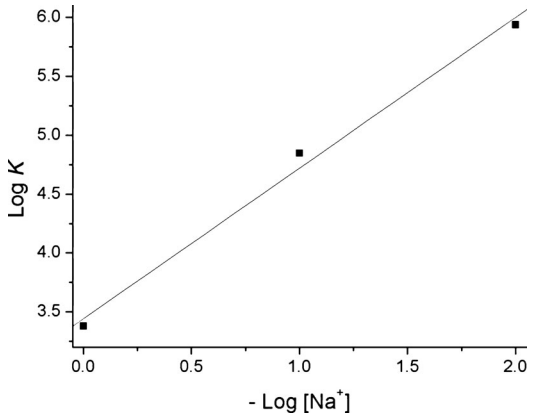

Figure 7. Dependence of the equilibrium constants on the salt concentration in the **1**·BF_4/CT-DNA system (pH 7.0, $T=25\,°C$).

obtained according to [Eq. (7)] reported by Manning, Record, and co-workers:[47]

$$\log K = m'\psi(-\log Na^+) + \log K_0 \quad (7)$$

where m' represents the number of phosphodiester residues occupied by one dye (**1**·BF_4) molecule and Ψ is the extent of the DNA charge shielded by the counterions. The y-intercept of the plot yields a value for log K_0, which was defined as the binding constant in the absence of electrostatic effects. In this case, log $K_0=3.44$ ($\Delta G_{nonel}=-4.69$ kcal mol^{-1}).

Assuming that $\Delta G=\Delta G_{el}+\Delta G_{nonel}$, we obtained $\Delta G_{el}=-1.92$ kcal mol^{-1}; this value is larger than typical values for intercalation, for which the nonelectrostatic (stacking) forces primarily contribute to the overall binding[42] (ca. $\Delta G_{nonel}=-5.70$ kcal mol^{-1} for the intercalation of platinum proflavine[42] and thiazole orange (TO)[48] into DNA). The resulting slope is $m'\Psi=1.28$, which is steeper than the characteristic value for intercalation (1.0).[42,45,49] Bearing in mind that $\Psi=0.88$,[50] then $m'=1.45$, that is, each dye molecule interacting with CT-DNA displaces 1.5 Na^+ ions. These results concurred with an external binding for mode 1 rather than intercalation.

Melting Experiments

At $I=0.1$ M, the melting curves were obtained for C_D/C_P ratios of 0–1, where C_D and C_P are the total **1**·BF_4 and CT-DNA concentrations, respectively; under such conditions, mode 2 binding predominated, as reflected in Figure 5B ($C_P/C_D>1$). The melting process can then be expressed as:

$$A_2 \overset{K_d}{\rightleftharpoons} 2A \quad (8)$$

The denaturation constant can be defined as $K_d=4C_0\alpha^2/(1-\alpha)$, where α is the fraction of single strands at each temperature and C_0. No appreciable change was observed in the melting profile and melting temperature when the C_D/C_P ratio was raised (Table 3); that is, at $I=0.1$ M, complex **1**·BF_4 did not contribute to the thermal stabilization of the double helix. The Supporting Information, Figure S5 shows the plot of ln K_d vs. $1/T$ in the vicinity of the melting point. The van't Hoff enthalpy (ΔH^0_{vH}) and entropy (ΔS^0_{vH}) values were calculated using Equation (9):[51]

$$\ln K_d = \frac{\Delta H^0}{R}\cdot\frac{1}{T}+\frac{\Delta S^0}{R} \quad (9)$$

Table 3. Thermodynamic parameters, T_m, ΔH^0_{vH}, ΔS^0_{vH}, and ΔG^0 for the **1**·BF_4/CT-DNA system at different C_D/C_P values, $C_P=3.0\times10^{-5}$ M, $I=0.1$ M, pH 7.0, $T=25\,°C$.

C_D/C_P	T_m [°C]	$\Delta H°_{vH}$ [kcal mol^{-1}]	$\Delta S°_{vH}$ [cal/K mol]	$\Delta G°$ [kcal mol^{-1}]
0	80.0	130	349	6.93
0.1	79.9	130	349	7.03
0.3	78.8	134	360	7.33
0.6	80.0	129	346	7.09
1.0	81.2	134	361	6.73

The van't Hoff ΔH^0_{vH}, ΔS^0_{vH}, and ΔG^0 values remained essentially constant over the whole C_D/C_P ratio range (Table 3). The binding mode of intercalation between stacked metal-complex cations and DNA is well-known to strongly stabilize its native conformation,[43,52,53] with a considerable increase in the melting temperature (T_m), contrary to the behavior observed here. By and large, intercalation results in a variation of thermodynamic parameters as a function of the C_D/C_P ratio.[54] Therefore, these features indicated that the mode 2 binding corresponded to off-slot binding.

Circular Dichroism

CD measurements were performed at the same three ionic strengths investigated in the fluorescence titrations: 0.01, 0.1, and 1.0 M (NaCl). The spectra showed changes in the DNA region (Figure 8). The negative band at 260 nm and the positive band at 275 nm both decreased in intensity as the C_D content was raised. These changes were more significant at low ionic strength. An induced circular dichroism effect appeared outside the DNA-absorption region; the small bands were ascribed to formation of the **1**·BF_4/CT-DNA complex, because neither DNA nor complex **1**·BF_4 displayed CD bands in this region. At the lowest ionic strength (0.01 M), there were two positive bands centered at 330 and 480 nm and a small negative band (375 nm) that displayed two isodicroic points (Figure 8A). These bands evolved upon raising the ionic strength; the positive band at 330 nm disappeared and turned into a negative, weaker band, with the added effect that the isodicroic point was missed (Figure 8B,C). This behavior suggested that the binding mode evolved as the ionic strength was increased. Figure 8D–F show the [θ] parameter at different ionic strengths as a function of the C_D/C_P ratio. The CD spectra evolved according to the observed changes in fluorescence (Figure 5), thus showing two branches at $I=0.01$ and 0.1 M, which correspond to modes 2 and 1, respectively, and only

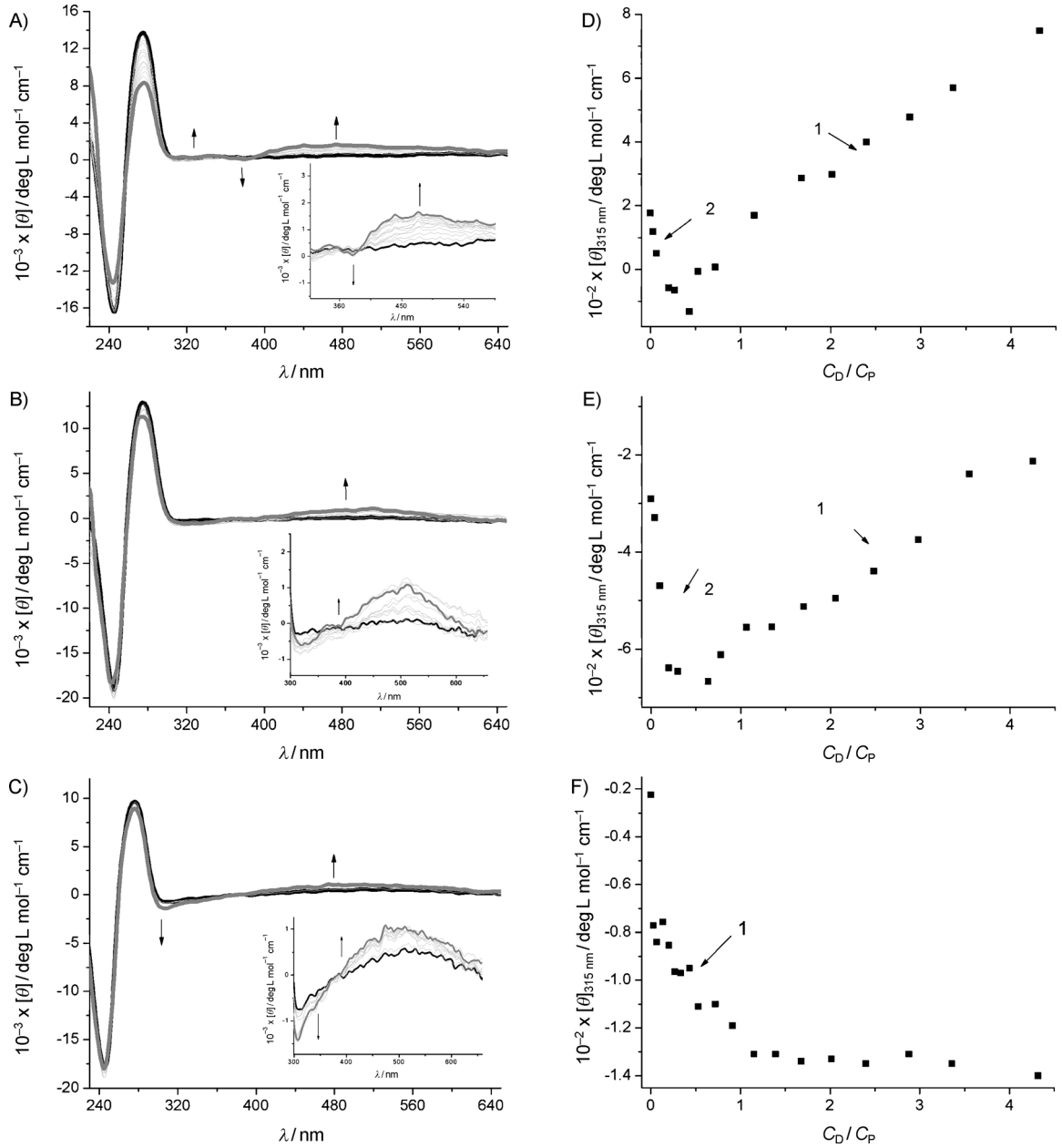

Figure 8. Circular dichroism spectra for the **1**·BF_4/CT-DNA system; $C_D/C_P = 0$–4, $C^0_P = 1.05 \times 10^{-4}$ M, pH 7.0, $T = 25$ °C. A) $I = 2.5$ mM, B) $I = 0.01$ M, C) $I = 0.1$ M, and D) $I = 1.0$ M. (D–F) plots [θ] vs. C_D/C_P at $\lambda = 315$ nm.

one branch at $I = 1.0$ M, which corresponds mostly to mode 1. Once again, the two binding modes were dependent on the ionic strength and on the C_D/C_P ratio.

Viscosity Measurements

At $I = 0.01$ M, the relative viscosity decreased as the C_D/C_P ratio was raised up to 2 (Figure 9). According to Cohen and Eisenberg,[55] the relative viscosity/contour-length relationship is of the form: $L\,L^{-1}{}_0 = (\eta/\eta_0)^{1/3}$, where L_0 and η_0 denote the apparent molecular length and solution viscosity in the absence of a metal complex, respectively. A rise in the relative viscosity reflected an increase in the apparent polymer length. These findings indicated that the **1**·BF_4 complex caused no elongation of the double helix and that the two modes of binding were compatible with external binding, because intercalation into DNA would result in an increase in the relative viscosity.[55–57] In other words, the reported intercalation of the triazine ligand was not found here.[20] The behavior of the molar ellipticity (Figure 8D) fit the viscosity measurements nicely. Two different branches were observed: the branch mode 2 for $C_D/C_P \leq 0.5$ and the mode 1 for $C_D/C_P > 0.5$. The small values deduced for the formation constants K_2 (Table 2) and the observed increase in fluorescence (Figure 5A) indicated that the binding mode 2 was merely electrostatic in nature and that the interaction came about through the *p*-cymene group, as previously de-

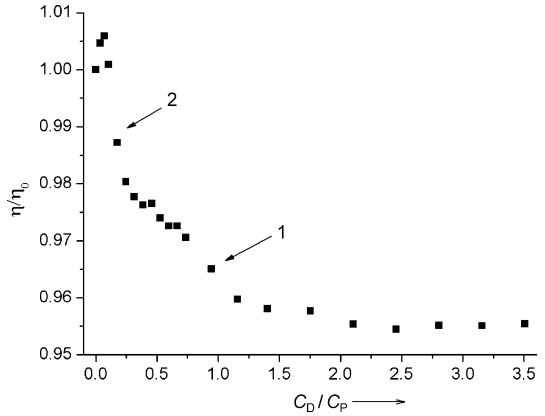

Figure 9. Relative viscosity of the **1**·BF_4/CT-DNA system; $C_D/C_P = 0$–3.5, $C^0_P = 2.37 \times 10^{-4}$ M, $I = 0.01$ M, pH 7.0, $T = 25$ °C.

scribed.[7,28,29] On the other hand, the functional groups of ligand 2-pydaT bound to the groove with rather high affinity, as revealed by the K_1 values (Table 2). This diminution in the viscosity (Figure 9) allowed us to conclude that complex **1**·BF_4 behaved as a bifunctional complex. The double interaction through the *p*-cymene and triazine groups brought about a small amount of DNA folding, which was perceivable by the shortening of the length of the double helix.

Cytotoxicity

The cytotoxicity of the PhdaT and 2-pydaT ligands and of the **1**·BF_4, **1**·TsO, and **2**·BF_4 Ru complexes were tested using 24 h incubation assays. The Supporting Information, Figure 6 shows the averaged survival percentages from at least two independent experiments with V79 cells from 0 to 1 mM (log scale). The survival percentage at the doses tested was similar relative to the negative control, thus indicating the absence of a dose-response relationship at those concentrations.

Genotoxicity

The genotoxic activity of complex **1**·BF_4 was tested using the cytokinesis-block micronucleus assay, which has been extensively applied to screen chemicals for potential genotoxicity. The MN/BN and %MNBN indices were plotted as functions of complex concentration, from 0–1 mM. The data for the doses tested were insignificant relative to the negative control (see the Supporting Information, Figure 7), thus suggesting that the Ru complex was not genotoxic.

Ru^{II} complexes containing Cl, triazine, or arene ligands are known to display antitumor activity. Hence, we expected that the complexes investigated herein, which contained all of these moieties, should display biological activity. However, they displayed neither genotoxic nor cytotoxic activity, even at high concentrations.

The NMR spectra in basic medium (Figure 4) confirmed the formation of the hydrolyzed Ru–OH complex (**5**) and the brown color in basic solution (see the Supporting Information, Figure 8) was also observed in cell assays. Hence, considering that Ru–OH bonds are considered to be biologically unreactive[6,21–23] we can conclude that the hydroxo complex was present in the cell medium.

Conclusions

2,4-Diamino-6-(2-pyridyl)-1,3,5-triazine (2-pydaT) can be used as a bidentate κ^2-*N*,*N* ligand to prepare new cationic arene–Ru^{II} complexes of the general formula [(η^6-arene)RuCl(κ^2-*N*,*N*-2-pydaT)]X (arene = *p*-cymene: **1**·X; arene = benzene: **2**·X). Furthermore, PhdaT was used to prepare the *ortho*-ruthenated complex [(η^6-*p*-cymene)RuCl(κ^2-C,N-PhdaT*)] (**3**). Crystal structures of both **1**·BF_4 and **3**·H_2O were determined by X-ray diffraction and displayed the typical features of these kind of complexes, along with an extensive network of H-bonding interactions through, among others, the NH_2 and Cl^- groups, and the counter-ion (BF_4^- in **1**·BF_4) or the solvent water molecule (**3**); π–π stacking, anion–π, and CH–π interactions were also found in the crystalline structure.

Complexes **1**·BF_4 and **3** took part in aquation/anation equilibria that were suppressed by the presence of NaCl; complexes **1**·BF_4 also underwent basic hydrolysis.

All of the data concurred in showing that the ruthenium complex **1**·BF_4, which was slightly fluorescent, interacted with DNA through two different modes: 1) an external groove binding (mode 1), with a large binding constant and a quenching effect by interaction with the 2-pydaT ligand; 2) by contrast, the slight electrostatic interaction led to a pronounced fluorescence increase when the C_P/C_D ratio was increased (mode 2; Figure 5A), that is, when the fluorophore concentration decreased. This feature may be ascribed to an electrostatic interaction between the DNA bases and the *p*-cymene ring. The viscosity decrease indicated that **1**·BF_4 behaved as a bifunctional complex and that the concurrent interaction through the *p*-cymene and triazine entities caused a small degree of DNA folding. Nevertheless, no relevant biological activity was observed. Thus, the basic hydrolysis reaction with the components of the cell-culture medium was the probable reason for the drug inactivation.

Experimental Section

Materials

Starting materials: [(η^6-arene)Ru(μ-Cl)Cl]$_2$ (arene = *p*-cymene, benzene),[32,33] [(η^6-C_6H_6)$RuCl_2(CH_3CN)$],[34] and ligands PhdaT[58] and 2-pydaT[59] were prepared according to literature procedures. $AgBF_4$, AgTsO, 2'-deoxyguanosine 5'-monophosphate free acid (dGMP), and Et_3N were purchased from Aldrich and used without further purification. Deuterated solvents were obtained from SDS and Euriso-top. Complex [(η^6-*p*-cymene)RuCl(κ^2-*N*,*N*-2-pydaT)]BF_4 (**1**·BF_4) may work as a drug and its concentration is referred to as C_D. The working solutions, made up by weight, were always freshly prepared. The aqueous solutions were prepared by using doubly deionized water from a Millipore Q apparatus (APS; Los Angeles, California). The ionic strength was adjusted with

NaCl. Sodium cacodylate buffer was used to keep the pH at a constant value of 7.0. Calf thymus DNA, purchased from Sigma Aldrich, was dissolved in water and sonicated using a MSE-Sonyprep sonicator by applying 20 cycles of 10 s sonication to suitable DNA samples (10 mL CT-DNA, 2×10^{-3} M) with 20 s pauses between cycles, at an amplitude of 98 μm. The sonicator tip was introduced directly into the solution, which was kept in an ice bath to minimize thermal sonication effects. The agarose gel electrophoresis tests indicated that the polymer length was reduced to approximately 1000 base-pair fragments. Stock solutions were standardized spectrophotometrically, using $\varepsilon=13200\,M^{-1}cm^{-1}$ at $\lambda=260$ nm,[60] $I=0.1$ M, 0.0975 M NaCl, 2.5 mM sodium cacodylate (NaCaC), pH 7.0. The DNA concentration, expressed as a molarity of the base-pair (M_{BP}), was referred to as C_p.

The (3-(4,5-dimethylthiazol-2-yl)-2,5-diphenyltetrazolium bromide (MTT) cytotoxicity and the cytokinesis-block micronucleus assays were performed in wild-type V79 Chinese hamster cells (MZ) that belonged to a widely used non-transformed mammalian cell-line devoid of CYP activity.[61] The cells were kindly provided by Prof. H. R. Glatt (German Institute of Human Nutrition).

General Methods

All synthetic manipulations were carried out under an atmosphere of dry oxygen-free nitrogen using standard Schlenk techniques. Solvents were distilled over their appropriate drying agents and degassed before use. Elemental analysis was performed with a Perkin–Elmer 2400 CHN microanalyzer. Analytical data were obtained from crystalline samples when possible. In some cases, the data were completely accurate, but in others the agreement between the calculated and observed values for carbon was >0.4%; therefore, solvent molecules were introduced into the molecular formulas to improve agreement. In any case, all of the complexes were obtained in high enough analytic purity to be used as starting materials. IR spectra were recorded on a Nicolet Impact 410 spectrophotometer as KBr pellets and on a Jasco (650–160 cm^{-1} range) as Nujol mulls deposited on a polyethylene film. FAB Mass spectra (position of the peaks in DA) were recorded with an Autospec spectrometer. NMR samples were prepared under a nitrogen atmosphere by dissolving the suitable amount of compound in 0.5 mL of the respective oxygen-free deuterated solvent and the spectra were recorded at 298 K (unless otherwise stated) on a Varian Unity Inova-400 (400 MHz for ^{1}H NMR, 161.9 MHz for ^{31}P NMR, and 100.6 MHz for ^{13}C NMR spectroscopy). Typically, 1D ^{1}H NMR spectra were acquired over 32 scans as 32 k data points over a spectral width of 16 ppm. ^{1}H and $^{13}C\{^1H\}$ NMR chemical shifts were internally referenced to trimethylsilyl (TMS) via 1,4-dioxane in D_2O ($\delta=3.75$ ppm and $\delta=67.19$ ppm respectively), or via the residual ^{1}H and ^{13}C NMR signals of the corresponding solvents (CD_3OD: $\delta=3.31$ and 49.00 ppm, $(CD_3)_2SO$: $\delta=2.50$ and 39.52 ppm), according to the values reported by Fulmer et al.[62] Chemical shift values are reported in ppm and coupling constants (J) in Hertz. The splitting of proton resonances in the ^{1}H NMR data is defined as s = singlet, d = doublet, t = triplet, q = quartet, sept = septet, m = multiplet, bs = broad singlet, pt = pseudo-triplet. All ^{31}P NMR resonances were referenced to 85% H_3PO_4 at 0 ppm. 2D spectra were recorded using standard pulse–pulse sequences. COSY spectra: standard pulse sequence, acquisition time 0.214 s, pulse width 10 μs, relaxation delay 1 s, 16 scans, 512 increments. The nOe difference spectra were recorded at 5000 Hz, acquisition time 3.27 s, pulse width 90°, relaxation delay 4 s, and irradiation power 5–10 dB. The probe temperature, (±1) K, was controlled by a standard unit calibrated with a MeOH reference. All NMR data processing was carried out using MestReNova version 6.1.1.

X-ray Crystallography

A summary of the crystal data collection and refinement parameters for all compounds is given in the Supporting Information, Table 4.

The single crystals for **2**·BF_4 and **3**·H_2O were mounted on a glass fiber and transferred into a Bruker X8 APEX II CCD-based diffractometer equipped with a graphite monochromated $Mo_{K\alpha}$ radiation source ($\lambda=0.71073$ Å). The highly redundant datasets were integrated using SAINT[63] and corrected for Lorentz and polarization effects. The absorption correction was based on fitting a function to the empirical transmission surface, as sampled by multiple equivalent measurements with the program SADABS.[64]

The software package SHELXTL version 6.10[65] was used for space-group determination, structure solution, and refinement by full-matrix least-squares methods based on F^2. A successful solution by the direct methods provided most non-hydrogen atoms from the E-map. The remaining non-hydrogen atoms were located in an alternating series of least-squares cycles and difference Fourier maps. All non-hydrogen atoms were refined with anisotropic displacement coefficients unless otherwise noted. Hydrogen atoms were placed using a "riding model" and were included in the refinement at calculated positions.

CCDC 850269 (**2**·BF_4) and CCDC 850270 (**3**·H_2O) contain the supplementary crystallographic data for this paper. These data can be obtained free of charge from the Cambridge Crystallographic Data Centre via www.ccdc.cam.ac.uk/data_request/cif.

pH Measurements

The pH values of NMR samples in D_2O were obtained at 298 K before and after recording the NMR spectra, using a Metrohm 16 DMS Titrino pH meter fitted out with a combined glass electrode and a 3 M KCl solution as a liquid junction, which was calibrated with Radiometer Analytical SAS buffer solutions at pH 1.679, 2.000, 4.005, 6.865, 7.000, and 7.413. No correction was applied for the effect of deuterium on the glass electrode.

Molar Conductivity Measurements

The Λ_M values are given in $S\,cm^2\,mol^{-1}$ and were obtained at room temperature for 10^{-3} M solutions of the corresponding complexes in CH_3CN, using a CRISON conductometer 522 equipped with a CRISON platinum conductivity cell 5292.

Aqueous-Solution Chemistry

The aquation–anation equilibrium and the basic hydrolysis of the Ru^{II}–chloro complex **1**·BF_4 were monitored by ^{1}H NMR spectroscopy. The spectra were recorded for 18 mM solutions in D_2O at various time intervals and the signals referenced to TMS via 1,4-dioxane as an internal reference ($\delta=3.75$ ppm). The relative amounts of the Ru^{II}–chloro complex and the aqua derivative were determined by integration of the respective ^{1}H resonances.

Spectrophotometric Studies

The thermal-denaturation assays and spectrophotometric studies were performed on a Hewlett–Packard 8453 A (Agilent Technologies, Palo Alto, California) spectrophotometer fitted out with diode-array detection and computer-assisted temperature-control systems. Thermal denaturation studies were carried out at $C_P=3.0\times10^{-5}$ M_{BP} and C_D/C_P ratios in the range 0–1. Titrations were performed by adding increasing amounts of DNA into a cell that contained a solution of complex **1**·BF_4 at an initial concentration of 2.0×10^{-5} M.

Fluorescence Titrations

The fluorescence titrations were performed on a Shimadzu Corporation RF-5301PC spectrofluorimeter (Duisburg, Germany) at $\lambda_{exc}=415$ nm and $\lambda_{em}=480$ nm. The titrations were carried out by adding increasing amounts of CT-DNA directly into the cell containing the dye solution. The CD spectra were recorded on a MOS-450 Bio-Logic spectrometer (Claix, France). The measurements were performed in cells of pathlength 1.0 cm at 25 °C; the titrations were performed by adding increasing microamounts of the dye to a known volume of the CT-DNA solution ($C_P=1.1\times10^{-4}$ M).

Viscosity Measurements

Viscosity measurements were performed on an Ubbelodhe viscometer (Schott, Mainz, Germany), which was immersed in a Julabo thermostated water bath that was maintained at 25.0(±0.1) °C. The flow time was measured with a digital stopwatch; mean values of triplicated measurements

CHEMISTRY
AN ASIAN JOURNAL

were used to evaluate the sample viscosity. To accurately analyze the viscosity measurements, two different assays were carried out: the first assay to estimate the role of the solvent ($I=1.0$ M (NaCl), pH 7.0 (sodium cacodylate), $T=25$ °C) in the DNA solution, and the second assay to evaluate the effect of complex **1**·BF_4 on the DNA; this procedure has enabled us to correct viscosity changes other than those stemming from **1**·BF_4/DNA interactions. The relative viscosity was calculated using the equation $\eta/\eta_0=\eta_{DNA/\mathbf{1}\cdot BF_4}/\eta_{DNA/solvent}$.

Cytotoxicity Assays

The MTT cytotoxicity assay was based on the reduction of the yellow MTT tetrazolium salt by mitochondrial dehydrogenases to form a blue MTT formazan in viable cells.[66] Approximately 7×10^3 V79 Chinese hamster cells were cultured in 200 µL culture medium per well (Ham's F-10 medium), supplemented with 10% newborn calf serum and 1% penicillin-streptomycin solution in 96-well plates and incubated at 37 °C under a 5% CO_2 atmosphere. The cells were grown for 24 h and then exposed to different concentrations of the Ru complexes (dissolved in the culture medium) for 24 h. Hydrogen peroxide was used as a positive control. The cells were washed with the culture medium and incubated with MTT (500 µg mL^{-1}) for a further 3 h. The medium was removed at the end of the incubation and the cells carefully washed with PBS. Afterward, 200 µL DMSO was added to each well. The absorbance was read at 595 nm in a Zenyth 3100 microplate reader. At least two independent experiments were performed with four replicates per dose.

Genotoxicity Assay

The cytokinesis-block micronucleus assay was performed as described previously,[67] with any modifications briefly described below. Approximately 7.6×10^5 V79 Chinese hamster cells were cultured in a culture medium (Ham's F-10 medium), which was supplemented with 10% newborn calf serum and 1% penicillin-streptomycin solution, and incubated at 37 °C under a 5% CO_2 atmosphere. The cells were grown for 24 h and then exposed to different concentrations of Ru complexes (dissolved in culture medium) for 24 h. Negative and positive controls (mytomicin-C at a final concentration of 2.5 µg mL^{-1}) were included. Afterwards, the medium was removed, the cells washed, and a fresh culture medium with cytochalasin-B (cyt-B) was added to afford a final concentration of 4.5 µg mL^{-1}.[68] The cells were grown for a further 16 h for the recovery of binucleated V79 cells. The cells were then harvested by trypsinization, rinsed, and subjected to mild hypotonic treatment, as described previously.[69] The centrifuged cells were placed on dry slides and smears were spread. After air-drying, the slides were fixed with MeOH at −20 °C (30 min). After 24 h, the slides were stained for 10 min with Giemsa (4% v/v in 0.01 M phosphate buffer, pH 7.0). For each experimental point, 1000 binucleated V79 cells (BN) with well-preserved cytoplasm were scored and micronuclei were identified according to the selection criteria,[68] using a 500× magnification on a light microscope. Two indices were evaluated: the MN/BN index, which represents the average number of micronuclei per binucleated cell, and the %MNBN index, which represents the cytokinesis-blocked (binucleated) cell fraction with micronuclei, regardless of the number of micronuclei per BN cell.

*General Procedure for the Synthesis of Complexes [(η^6-p-cymene)RuCl(κ^2-N,N-2-pydaT)]X, (**1**·BF_4), and (**1**·TsO)*

[{(η^6-*p*-cymene)Ru(µ-Cl)Cl}$_2$] (0.16 mmol) was stirred for 30 min with either $AgBF_4$ or AgTsO (0.32 mmol) in degassed EtOH (30 mL) at room temperature in a darkened Schlenk tube. Then, compound 2-pydaT (0.32 mmol) was added and the mixture was stirred overnight at room temperature. AgCl was removed by filtration under an inert atmosphere and the solvent was evaporated to dryness. The solid residue was washed with *n*-hexane (2×10 mL), and dried under vacuum to produce a yellow solid.

*[(η^6-p-cymene)RuCl(κ^2-N,N-2-pydaT)]BF_4 (**1**·BF_4)*

The amounts were as follows: [{(η^6-*p*-cymene)Ru(µ-Cl)Cl}$_2$] (100 mg, 0.16 mmol), $AgBF_4$ (63.2 mg, 0.32 mmol), 2-pydaT (61.1 mg, 0.32 mmol).

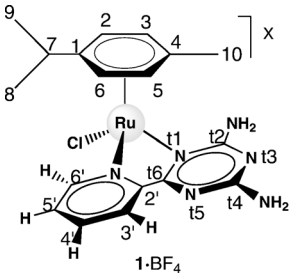

1·BF_4

X=BF_4 (**1**·BF_4)

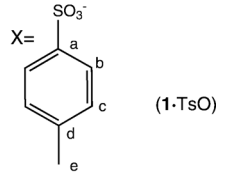

(**1**·TsO)

Yellow solid; yield: 132.4 mg (0.24 mmol, 74.8%); ^{1}H NMR (400 MHz, CD_3OD): $\delta=9.37$ (m, 1H; pyH$^{6'}$), 8.45 (m, 1H; pyH$^{3'}$), 8.23 (td, $J=7.8$, 1.4 Hz, 1H; pyH$^{4'}$), 7.86 (ddd, $J=7.3$, 5.6, 1.5 Hz, 1H; pyH$^{5'}$), 6.14 (d, $^3J=6.1$ Hz, 1H; cymH^2), 5.92 (sq, $^3J=6.5$ Hz, 2H; cymH^{5,6}), 5.80 (d, $^3J=6.1$ Hz, 1H; cymH^3), 2.58 (sept, $^3J=6.9$ Hz, 1H; cymH^7), 2.30 (s, 3H; cymH^{10}), 1.12 (d, $^3J=6.9$ Hz, 3H; cymH^8), 1.00 ppm (d, $^3J=6.9$ Hz, 3H; cymH^9); ^{1}H NMR (400 MHz, CD_3SOCD_3): $\delta=9.45$ (m, 1H; pyH^6), 8.42 (bs, 2H; NH_2), 8.29 (m, 1H; pyH), 7.92 (m, 2H; pyH), 6.28 (bs, 2H; NH_2), 6.16 (m, 1H; cymH), 6.06 (m, 1H; cymH), 6.00 (m, 1H; cymH), 2.54 (sept, $^3J=6.9$ Hz, 1H; cymH^7), 2.22 (s, 3H; cymH^{10}), 1.03 (d, $^3J=6.9$ Hz, 3H; cymH^8), 0.90 ppm (d, $^3J=6.9$ Hz, 3H; cymH^9); ^{13}C NMR (101 MHz, CD_3OD): $\delta=169.73$ (s, 1C; tzC^{t6}), 167.48 (s, 1C; tzC^{t2}), 167.27 (s, 1C; tzC^{t4}), 157.02 (s, 1C; pyC$^{6'}$), 154.67 (s, 1C; pyC$^{2'}$), 141.23 (s, 1C; pyC$^{4'}$), 131.09 (s, 1C; pyC$^{5'}$), 127.23 (s, 1C; pyC$^{3'}$), 106.14 (s, , 1C; cymC^4), 105.43 (s, 1C; cymC^1), 87.61 (s, 1C; cymC^6), 86.72 (s, 1C; cymC^2), 84.40 (s, 1C; cymC^5), 83.50 (s, 1C; cymC^3), 32.36 (s, 1C; cymC^7), 22.40 (s, 1C; cymC^8), 22.21 (s, 1C; cymC^9), 18.96 ppm (s, 1C; cymC^{10}); ^{19}F NMR (376 MHz, CD_3OD): $\delta=-154.83$ (s; ^{10}B-F), −154.88 ppm (s; ^{11}B-F); IR (KBr): $\tilde{\nu}=3196$, 2971, 2963, 1619, 1510, 1083, 784, 521 cm^{-1}; IR (nujol): $\tilde{\nu}=376$, 303, 279, 247, 228, 222, 213, 201, 194, 180, 171, 162 cm^{-1}; MS (FAB, MeOH): *m/z*: 459 [*M*−BF_4]$^+$, 325 [*M*−BF_4−cym]$^+$; molar conductivity (CH_3CN): 200 S cm^2 mol^{-1}; solubility: soluble in MeOH, EtOH, and water; M_r ($C_{18}H_{22}N_6ClRuBF_4$): 545.7386 g mol^{-1}; elemental analysis calcd (%) for $C_{18}H_{22}N_6ClRuBF_4$·3/2CH_3OH: C 41.02, H 5.08, N 13.67; found: C 41.16, H 4.84, N 13.32.

*Synthesis of [(η^6-p-cymene)RuCl(κ^2-N,N-2-pydaT)]OTs (**1**·TsO)*

The amounts were as follows: [{(η^6-*p*-cymene)Ru(µ-Cl)Cl}$_2$] (100 mg, 0.16 mmol), AgTsO (90.5 mg, 0.32 mmol), 2-pydaT (61.1 mg, 0.32 mmol). Yellow solid; yield: 178.5 mg (0.28 mmol, 87.3%); ^{1}H NMR (400 MHz, CD_3OD): $\delta=9.37$ (m, 1H; pyH$^{6'}$), 8.44 (m, 1H; pyH$^{3'}$), 8.22 (td, $J=7.8$, 1.4 Hz, 1H; pyH$^{4'}$), 7.84 (ddd, $J=7.7$, 5.6, 1.6 Hz, 1H; pyH$^{5'}$), 7.72 (d, ^3J-(H,H)=8.1 Hz, 2H; H^b-TsO$^-$), 7.23 (d, $^3J_{HH}=8.1$ Hz, 2H; H^c-TsO$^-$), 6.13 (d, $^3J=6.1$ Hz, 1H; cymH^2), 5.91 (m, 2H; cymH^{5,6}), 5.79 (d, $^3J=6.1$ Hz, 1H; cymH^3), 2.57 (sept, $^3J=6.9$ Hz, 1H; cymH^7), 2.36 (s, 3H; H^e-TsO$^-$), 2.29 (s, 3H; cymH^{10}), 1.11 (d, $^3J=6.9$ Hz, 3H; cymH^8), 1.00 ppm (d, $^3J=6.9$ Hz, 3H; cymH^9); ^{13}C NMR (101 MHz, CD_3OD): $\delta=169.71$ (s, 1C; tzC^{t6}), 167.50 (s, 1C; tzC^{t2}), 167.27 (s, 1C; tzC^{t4}), 156.97 (s, 1C; pyC$^{6'}$), 154.72 (s, 1C; pyC$^{2'}$), 143.56 (s, 1C; C^a-TsO$^-$), 141.65 (s, 1C; C^d-TsO$^-$), 141.23 (s, 1C; pyC$^{4'}$), 131.02 (s, 1C; pyC$^{5'}$), 129.82 (s, 1C; C^c-TsO$^-$), 127.24 (s, 1C; pyC$^{3'}$), 126.97 (s, 1C; C^b-TsO$^-$), 106.19 (s, 1C; cymC^4), 105.37 (s, 1C; cymC^1), 87.61 (s, 1C; cymC^6), 86.74 (s, 1C; cymC^2), 84.35 (s, 1C; cymC^5), 83.46 (s, 1C; cymC^3), 32.36 (s, 1C; cymC^7), 22.42 (s, 1C; cymC^8), 22.22 (s, 1C; cymC^9), 21.33 (s, 1C; C^e-TsO$^-$), 18.97 (s, 1C; cymC^{10}); IR (KBr): 3445, 3215, 3064, 2967, 1634, 1188, 784, 683, 567 cm^{-1}; IR (nujol): 292, 261, 252, 214, 176, 172, 162 cm^{-1}; MS (FAB, MeOH): *m/z*: 459 ([*M*−TsO]$^+$, 325 ([*M*−TsO−cym]$^+$; molar conductivity (CH_3CN): 89.4 S cm^2 mol^{-1}; solubility: soluble in MeOH, EtOH, and water; M_r ($C_{25}H_{29}N_6ClSO_3Ru$): 630.1255 g mol^{-1}; elemental analysis calcd (%) for $C_{25}H_{29}N_6ClSO_3Ru$·CH_3OH: C 47.96, H 5.22, N 12.43, S 4.74; found: C 47.78, H 5.17, N 11.94, S 4.64.

*General Procedure for the synthesis of complexes [(η^6-benzene)RuCl(κ^2-N,N-2-pydaT)]X, (**2**·BF_4), and (**2**·TsO)*

A solution of [$RuCl_2(C_6H_6)(CH_3CN)$] (0.34 mmol) in a degassed mixture of CH_3CN/MeOH (10 mL:10 mL) was stirred for 2 h with $AgBF_4$

(0.34 mmol) at room temperature in a darkened Schlenk tube. AgCl was removed by filtration under an inert atmosphere. Then, compound 2-pydaT (0.34 mmol) was added and the mixture was stirred at room temperature for 24 h. The solvent was removed under vacuum. The solid residue was washed with Et_2O (2×10 mL), and dried under vacuum to produce a yellow solid.

*[(η^6-benzene)RuCl(κ^2-N,N-2-pydaT)]BF_4 (**2**·BF_4)*

Amounts were as follows: [$RuCl_2(C_6H_6)(CH_3CN)$] (100 mg, 0.34 mmol), $AgBF_4$ (66.2 mg, 0.34 mmol), 2-pydaT (64.5 mg, 0.34 mmol). Yellow solid; yield: 122.41 mg (0.25 mmol, 73.5%); ^{1}H NMR (400 MHz, CD_3OD): δ = 9.47 (m, 1H; pyH$^{6'}$), 8.45 (dd, J = 8.1, 1.1 Hz, 1H; pyH$^{3'}$), 8.24 (td, 1H; pyH$^{4'}$), 7.85 (m, 1H; pyH$^{5'}$), 6.11 ppm (s, 6H; CH-bz); ^{13}C NMR (101 MHz, CD_3OD): δ = 169.87 (s, 1C; tzC^{t6}), 167.50 (s, 1C; tzC^{t2}), 167.36 (s, 1C; tzC^{t4}), 157.05 (s, 1C; pyC$^{6'}$), 155.19 (s, 1C; pyC$^{2'}$), 141.32 (s, 1C; pyC$^{4'}$), 130.91 (s, 1C; pyC$^{5'}$), 127.17 (s, 1C; pyC$^{3'}$), 87.94 ppm (s, 6C; bz); ^{19}F NMR (376 MHz, CD_3OD): δ = −155.34 (s; ^{10}B-F), −155.39 ppm (s; ^{11}B-F); IR (KBr): $\tilde{\nu}$ = 3433, 3219, 3091, 2928, 1634, 1503, 1068, 784 cm^{-1}; IR (nujol): $\tilde{\nu}$ = 443, 303, 289, 278, 252, 223, 202, 194, 177 cm^{-1}; MS (FAB, MeOH): m/z: 403 [$M-BF_4$]$^+$, 325 [$M-BF_4-C_6H_6$]$^+$; molar conductivity (CH_3CN): 138.5 s cm^2 mol^{-1}; solubility: barely soluble in MeOH and water; M_r ($C_{14}H_{14}N_6ClRuBF_4$): 489.6314 g mol^{-1}; elemental analysis calcd (%) for $C_{14}H_{14}N_6ClRuBF_4$: C 34.34, H 2.88, N 17.16; found: C 34.20, H 2.976, N 17.32.

*[(η^6-C_6H_6)RuCl(κ^2-N,N-2-pydaT)]TsO (**2**·TsO)*

Amounts were as follows: [$RuCl_2(C_6H_6)(CH_3CN)$] (100 mg, 0.34 mmol), $AgBF_4$ (95.7 mg, 0.34 mmol), 2-pydaT (64.5 mg, 0.34 mmol). Yellow solid; yield: 163.5 mg (0.29 mmol, 85.3%); ^{1}H NMR (400 MHz, CD_3OD): δ = 9.46 (m, 1H; pyH$^{6'}$), 8.43 (m, 1H; pyH$^{3'}$), 8.22 (m, 1H; pyH$^{4'}$), 7.84 (m, 1H; pyH$^{5'}$), 7.71 (d, ^3J(H,H) = 8.1 Hz, 2H; H^b-TsO$^-$), 7.23 (d, ^3J(H,H) = 8.1 Hz, 2H; H^c-TsO$^-$), 6.09 (s, 6H; CH-bz), 2.36 ppm (s, 3H; H^e-TsO$^-$); ^{13}C NMR (101 MHz, CD_3OD): δ = 169.87 (s, 1C; tzC^{t6}), 167.46 (s, 1C; tzC^{t2}), 167.36 (s, 1C; tzC^{t4}), 156.96 (s, 1C; pyC$^{6'}$), 155.15 (s, 1C; pyC$^{2'}$), 143.62 (s, 1C; C^a-TsO$^-$), 141.64 (s, 1C; C^d-TsO$^-$), 141.24 (s, 1C; pyC$^{4'}$), 130.85 (s, 1C; pyC$^{5'}$), 129.81 (s, 2C; C^c-TsO$^-$), 127.14 (s, 1C; pyC$^{3'}$), 126.97 (s, 2C; C^b-TsO$^-$), 87.81 (s, 6C; bz), 21.30 ppm (s, 1C; C^e-TsO$^-$); IR (KBr): $\tilde{\nu}$ = 3432, 3206, 3078, 2930, 1633, 1626, 1588, 1566, 1515, 1488, 1439, 1399, 1284, 1213, 1188, 1122, 1061, 1034, 1010, 848, 817, 786, 759, 684, 631, 616, 568 cm^{-1}; IR (nujol): $\tilde{\nu}$ = 496, 485, 446, 436, 289, 277, 251, 223, 207,198, 171, 166, 158 cm^{-1}; MS (FAB, MeOH): m/z: 403 [$M-BF_4$]$^+$, 325 [$M-BF_4-C_6H_6$]$^+$; molar conductivity (CH_3CN): 105.7 s cm^2 mol^{-1}; solubility: soluble in MeOH, EtOH, and water, and barely soluble in acetone and CH_2Cl_2; M_r ($C_{21}H_{21}N_6ClRuSO_3$): 574.02 g mol^{-1}; elemental analysis calcd (%) for $C_{21}H_{21}N_6ClRuSO_3$: C 43.94, H 3.69, N 14.64, S 5.59; found: C 43.56, H 3.53, N 14.39, S 5.73.

[(η^6-p-cymene)RuCl(κ^2-N,C-PhdaT)] (**3**)*

A solution of [{$RuCl_2$(*p*-cymene)}$_2$] (100 mg, 0.16 mmol) in degassed MeOH (30 mL) was stirred with PhdaT (60.7 mg, 0.32 mmol) and Et_3N (22 mg, 0.2 mmol) for 24 h under a nitrogen atmosphere at room temperature. Then, an additional amount of Et_3N (22 mg, 0.2 mmol) was added and the mixture was stirred for a further 24 h at room temperature. The resulting suspension was filtered to remove a dark residue and the filtrate was stirred under vacuum to reduce the volume to approximately 5 mL. Et_2O (10 mL) was added to precipitate a yellow–brown solid. The solid was isolated by filtration, washed with *n*-hexane (2×10 mL), and dried under vacuum to afford a yellow solid. Finally, the product was crystallized by slow evaporation from a solution in MeOH as a light brown solid. Yield: 28.4 mg (0.06 mmol, 19.4%); ^{1}H NMR (400 MHz, CD_3OD): δ = 8.14 (d, ^3J(H,H) = 7.2 Hz, 1H; Ph*H$^{6'}$), 7.83 (d, ^3J(H,H) = 7.9 Hz, 1H; Ph*H$^{3'}$), 7.23 (td, J = 7.6, 1.5 Hz, 1H; Ph*H$^{4'}$), 7.00 (td, J = 7.6, 1.5 Hz, 1H; Ph*H$^{5'}$), 5.73 (d, J = 6.0 Hz, 1H; cymCH), 5.58 (t, J = 5.4 Hz, 2H; cymCH), 5.24 (d, J = 5.4 Hz, 1H; cymCH), 2.20 (sept, 1H; cymH^7), 2.01 (s, 3H; cymH^{10}), 0.91 ppm (pt, 6H; cymH^{8,9}); IR (KBr): $\tilde{\nu}$ = 3364 (NH_2), 3303 (NH_2), 3197, 2963, 1622, 1566, 1551, 1510, (C=C and N=C), 1468, 1448, 1389, 1296, 1270, 1153, 1031, 817, 776, 733, 584, 503, 420 cm^{-1}; MS (FAB, MeOH): m/z: 496 [M+K]$^+$, 457 [M]$^+$, 422 [$M-$Cl]$^+$; solubility: barely soluble in MeOH and water; elemental analysis calcd (%) for $C_{19}H_{22}N_5ClRu{\cdot}H_2O$: C 48.05, H 5.09, N 14.75; found: C 48.16, H 5.02, N 14.59.

NMR Spectroscopic Data for Compound 2-pydaT

^{1}H NMR (400 MHz, CD_3OD): δ = 8.70 (m, 1H; pyH$^{6'}$), 8.38 (m, 1H; pyH$^{3'}$), 7.95 (m, 1H; pyH$^{4'}$), 7.55 ppm (m, 1H; pyH$^{5'}$).

*NMR Spectroscopic Data for Complex [(η^6-p-cymene)Ru(OH_2)(κ^2-N,N-2-pydaT)]$(BF_4)_2$ (**4**·$(BF_4)_2$)*

^{1}H NMR (400 MHz, D_2O): δ = 9.54 (m, 1H; pyH$^{6'}$), 8.48 (m, 1H; pyH$^{3'}$), 8.32 (m, 1H; pyH$^{4'}$), 7.97 (m, 1H; pyH$^{5'}$), 6.40 (d, ^3J = 6.2 Hz, 1H; cymH^2), 6.14 (m, 2H, cymH^{5,6}), 6.01 (d, ^3J = 6.2 Hz, 1H; cymH^3), 2.49 (sept, ^3J = 6.9 Hz, 1H; cymH^7), 2.26 (s, 3H; cymH^{10}), 1.04 (d, ^3J = 6.8 Hz, 3H; cymH^8), 0.93 ppm (d, ^3J = 6.9 Hz, 3H; cymH^9); ^{13}C NMR (101 MHz, D_2O): δ = 170.42 (s, 1C; tzC^{t6}), 166.24 (s, 1C; tzC^{t2}), 166.06 (s, 1C; tzC^{t4}), 156.26 (s, 1C; pyC$^{6'}$), 153.65 (s, 1C; pyC$^{2'}$), 142.20 (s, 1C; pyC$^{4'}$), 131.52 (s, 1C; pyC$^{5'}$), 127.57 (s, 1C; pyC$^{3'}$), 105.96 (s, 1C; cymC^4), 100.26 (s, 1C; cymC^1), 87.46 (s, 2C; cymC^{6,2}), 83.29 (s, 1C; cymC^5), 81.76 (s, 1C; cymC^3), 31.02 (s, 1C; cymC^7), 21.93 (s, 1C; cymC^8), 21.51 (s, 1C; cymC^9), 18.22 ppm (s, 1C; cymC^{10}).

*NMR Spectroscopic Data for Complex [(η^6-p-cymene)Ru(OH)(κ^2-N,N-2-pydaT)](BF_4) (**5**·BF_4)*

^{1}H NMR (400 MHz, D_2O): δ = 9.34 (d, J = 5.5 Hz, 1H; pyH$^{6'}$), 8.43 (d, J = 7.3 Hz, 1H; pyH$^{3'}$), 8.24 (m, 1H; pyH$^{4'}$), 7.88 (m, 1H; pyH$^{5'}$), 6.16 (d, J = 5.9 Hz, 1H; cymCH), 5.88 (d, J = 5.9 Hz, 2H; cymCH), 5.70 (d, J = 6.1 Hz, 2H; cymCH), 5.63 (d, J = 6.1 Hz, 1H; cymCH), 2.44 (sept, ^3J = 6.9 Hz, 1H; cymH^7), 2.29 (s, 3H; cymH^{10}), 0.97 (d, ^3J = 6.9 Hz, 3H; cymH^8), 0.85 ppm (d, ^3J = 6.9 Hz, 3H; cymH^9); ^{13}C NMR (101 MHz, D_2O): δ = 170.35 (s, 1C; tzC^{t6}), 166.33 (s, 1C; tzC^{t2}), 166.14 (s, 1C; tzC^{t4}), 155.70 (s, 1C; pyC$^{6'}$), 153.27 (s, 1C; pyC$^{2'}$), 141.13 (s, 1C; pyC$^{4'}$), 130.91 (s, 1C; pyC$^{5'}$), 126.92 (s, 1C; pyC$^{3'}$), 107.88 (s, 1C; cymC^4), 101.95 (s, 1C; cymC^1), 88.30 (s, 1C; cymCH), 86.80 (s, 1C; cymCH), 79.58 (s, 1C; cymCH), 78.25 (s, 1C; cymCH), 30.95 (s, 1C; cymC^7), 22.38 (s, 1C; cymC^8), 21.77 (s, 1C; cymC^9), 18.06 ppm (s, 1C; cymC^{10}).

Acknowledgements

The authors acknowledge financial support by the MICINN of Spain (CTQ2009-13051/BQU and CTQ2011-24434 supported by FEDER), the Junta de Castilla y León, (BU-013A-09, GR257, and GR78), and the University of Burgos, with funding by Caja de Burgos, Spain. We also thank the Portuguese Fundação da Ciência e Tecnologia (PTDC/QUI/67522/2006 and PTDC/QUI/66507/2006). Funding from the University of Pisa to promote international academic cooperation is also gratefully acknowledged. We are also grateful to the PCI of the University of Burgos for their technical support.

[1] F. Arnesano, G. Natile, *Coord. Chem. Rev.* **2009**, *253*, 2070.
[2] J. A. Gottlieb, B. Drewinko, *Cancer Chemother. Rep. Part 1* **1975**, *59*, 621.
[3] H. C. Harder, B. Rosenberg, *Int. J. Cancer* **1970**, *6*, 207.
[4] L. Ronconi, P. J. Sadler, *Coord. Chem. Rev.* **2007**, *251*, 1633.
[5] L. Dadci, H. Elias, U. Frey, A. Hornig, U. Koelle, A. E. Merbach, H. Paulus, J. S. Schneider, *Inorg. Chem.* **1995**, *34*, 306.
[6] H. M. Chen, J. A. Parkinson, R. E. Morris, P. J. Sadler, *J. Am. Chem. Soc.* **2003**, *125*, 173.
[7] R. E. Morris, R. E. Aird, P. D. Murdoch, H. M. Chen, J. Cummings, N. D. Hughes, S. Parsons, A. Parkin, G. Boyd, D. I. Jodrell, P. J. Sadler, *J. Med. Chem.* **2001**, *44*, 3616.
[8] R. E. Aird, J. Cummings, A. A. Ritchie, M. Muir, R. E. Morris, H. Chen, P. J. Sadler, D. I. Jodrell, *Br. J. Cancer* **2002**, *86*, 1652.
[9] S. H. van Rijt, P. J. Sadler, *Drug Discovery Today* **2009**, *14*, 1089.

[10] A. M. Pizarro, P. J. Sadler, *Biochimie* **2009**, *91*, 1198.
[11] W. H. Ang, A. Casini, G. Sava, P. J. Dyson, *J. Organomet. Chem.* **2011**, *696*, 989.
[12] M. J. Clarke, *Coord. Chem. Rev.* **2003**, *236*, 207.
[13] G. Süss-Fink, *Dalton Trans.* **2010**, *39*, 1673.
[14] A. Bergamo, G. Sava, *Dalton Trans.* **2007**, 1267.
[15] H. A. Wee, P. J. Dyson, *Eur. J. Inorg. Chem.* **2006**, 4003.
[16] G. S. Smith, B. Therrien, *Dalton Trans.* **2011**, *40*, 10793.
[17] Z. Hu, T. Ma, Z. Chen, Z. Q. Ye, G. L. Zhang, Y. J. Lou, Y. P. Yu, *J. Comb. Chem.* **2009**, *11*, 267.
[18] F. Sączewski, A. Bułakowska, P. Bednarski, R. Grunert, *Eur. J. Med. Chem.* **2006**, *41*, 219.
[19] F. Sączewski, A. Bułakowska, *Eur. J. Med. Chem.* **2006**, *41*, 611.
[20] C. Avendaño, J. C. Menéndez, *Medicinal Chemistry of Anticancer Drugs*, Elsevier, **2008**.
[21] M. H. Garcia, T. S. Morais, P. Florindo, M. F. M. Piedade, V. Moreno, C. Ciudad, V. Noe, *J. Inorg. Biochem.* **2009**, *103*, 354.
[22] F. Linares, M. A. Galindo, S. Galli, M. A. Romero, J. A. R. Navarro, E. Barea, *Inorg. Chem.* **2009**, *48*, 7413.
[23] F. Wang, H. M. Chen, S. Parsons, L. D. H. Oswald, J. E. Davidson, P. J. Sadler, *Chem. Eur. J.* **2003**, *9*, 5810.
[24] C. Gossens, A. Dorcier, P. J. Dyson, U. Rothlisberger, *Organometallics* **2007**, *26*, 3969.
[25] C. Scolaro, C. G. Hartinger, C. S. Allardyce, B. K. Keppler, P. J. Dyson, *J. Inorg. Biochem.* **2008**, *102*, 1743.
[26] M. Brindell, D. Piotrowska, A. A. Shoukry, G. Stochel, R. van Eldik, *J. Biol. Inorg. Chem.* **2007**, *12*, 809.
[27] S. R. Grguric-Sipka, R. A. Vilaplana, J. M. Perez, M. A. Fuertes, C. Alonso, Y. Alvarez, T. J. Sabo, F. Gonzalez-Vilchez, *J. Inorg. Biochem.* **2003**, *97*, 215.
[28] O. Novakova, H. M. Chen, O. Vrana, A. Rodger, P. J. Sadler, V. Brabec, *Biochemistry* **2003**, *42*, 11544.
[29] H. K. Liu, F. Wang, J. A. Parkinson, J. Bella, P. J. Sadler, *Chem. Eur. J.* **2006**, *12*, 6151.
[30] A. Casini, C. Gabbiani, F. Sorrentino, M. P. Rigobello, A. Bindoli, T. J. Geldbach, A. Marrone, N. Re, C. G. Hartinger, P. J. Dyson, L. Messori, *J. Med. Chem.* **2008**, *51*, 6773.
[31] S. J. Dougan, A. Habtemariam, S. E. McHale, S. Parsons, P. J. Sadler, *Proc. Natl. Acad. Sci. USA* **2008**, *105*, 11628.
[32] R. A. Zelonka, M. C. Baird, *Can. J. Chem.* **1972**, *50*, 3063.
[33] M. A. Bennett, A. K. Smith, *J. Chem. Soc. Dalton Trans.* **1974**, 233.
[34] H. Takahashi, K. Kobayashi, M. Osawa, *Anal. Sci.* **2000**, *16*, 777.
[35] C. Ganter, *Chem. Soc. Rev.* **2003**, *32*, 130.
[36] D. Zuccaccia, A. Macchioni, *Organometallics* **2005**, *24*, 3476.
[37] J. P. Djukic, A. Berger, M. Duquenne, M. Pfeffer, A. de Cian, N. Kyritsakas-Gruber, J. Vachon, J. Lacour, *Organometallics* **2004**, *23*, 5757.
[38] M. C. Carrión, F. Sepúlveda, F. A. Jalon, B. R. Manzano, A. M. Rodríguez, *Organometallics* **2009**, *28*, 3822.
[39] X. F. Wu, J. K. Liu, D. Di Tommaso, J. A. Iggo, C. R. A. Catlow, J. Bacsa, J. L. Xiao, *Chem. Eur. J.* **2008**, *14*, 7699.
[40] S. K. Singh, S. Joshi, A. R. Singh, J. K. Saxena, D. S. Pandey, *Inorg. Chem.* **2007**, *46*, 10869.
[41] H. A. Wee, E. Daldini, C. Scolaro, R. Scopelliti, L. Juillerat-Jeanneret, P. J. Dyson, *Inorg. Chem.* **2006**, *45*, 9006.
[42] T. Biver, F. Secco, M. R. Tine, M. Venturini, *Arch. Biochem. Biophys.* **2003**, *418*, 63.
[43] T. Biver, C. Cavazza, F. Secco, M. Venturini, *J. Inorg. Biochem.* **2007**, *101*, 461.
[44] X. L. Hong, H. Li, C. H. Peng, *J. Mol. Struct.* **2011**, *990*, 197.
[45] R. Ruiz, B. García, J. García-Tojal, N. Busto, S. Ibeas, J. M. Leal, C. Martins, J. Gaspar, J. Borras, R. Gil-García, M. González-Alvárez, *J. Biol. Inorg. Chem.* **2010**, *15*, 515.
[46] F. J. Meyer-Almes, D. Porschke, *Biochemistry* **1993**, *32*, 4246.
[47] M. T. Record, C. F. Anderson, T. M. Lohman, *Q. Rev. Biophys.* **1978**, *11*, 103.
[48] T. Biver, A. Boggioni, F. Secco, E. Turriani, M. Venturini, S. Yarnaoluk, *Arch. Biochem. Biophys.* **2007**, *465*, 90.
[49] D. P. Mascotti, T. M. Lohman, *Proc. Natl. Acad. Sci. USA* **1990**, *87*, 3142.
[50] T. Schelhorn, S. Kretz, H. W. Zimmermann, *Cell. Mol. Biol.* **1992**, *38*, 345.
[51] J. L. Mergny, L. Lacroix, *Oligonucleotides* **2003**, *13*, 515.
[52] A. Silvestri, G. Barone, G. Ruisi, M. T. Lo Giudice, S. Tumminello, *J. Inorg. Biochem.* **2004**, *98*, 589.
[53] D. J. Patel, *Acc. Chem. Res.* **1979**, *12*, 118.
[54] B. García, J. M. Leal, R. Ruiz, T. Biver, F. Secco, M. Venturini, *J. Phys. Chem. B* **2010**, *114*, 8555.
[55] G. Cohen, H. Eisenberg, *Biopolymers* **1969**, *8*, 45.
[56] D. Suh, Y. K. Oh, J. B. Chaires, *Process Biochem.* **2001**, *37*, 521.
[57] D. Suh, J. B. Chaires, *Bioorg. Med. Chem.* **1995**, *3*, 723.
[58] R. Deans, G. Cooke, V. M. Rotello, *J. Org. Chem.* **1997**, *62*, 836.
[59] F. H. Case, E. Koft, *J. Am. Chem. Soc.* **1959**, *81*, 905.
[60] M. E. Reichmann, S. A. Rice, C. A. Thomas, P. Doty, *J. Am. Chem. Soc.* **1954**, *76*, 3047.
[61] H. Glatt, H. Schneider, Y. G. Liu, *Mutat. Res. Genet. Toxicol. Environ. Mutagen.* **2005**, *580*, 41.
[62] G. R. Fulmer, A. J. M. Miller, N. H. Sherden, H. E. Gottlieb, A. Nudelman, B. M. Stoltz, J. E. Bercaw, K. I. Goldberg, *Organometallics* **2010**, *29*, 2176.
[63] SAINT+ v7.12a. Area-Detector Integration Program. Bruker-Nonius AXS. Madison, Wisconsin, USA, **2004**.
[64] G. M. Sheldrick, SADABS version 2004/1. A Program for Empirical Absorption Correction. University of Göttingen, Göttingen, Germany, **2004**.
[65] SHELXTL-NT version 6.12. Structure Determination Package. Bruker-Nonius AXS. Madison, Wisconsin, USA, **2001**.
[66] J. Carmichael, W. G. Degraff, A. F. Gazdar, J. D. Minna, J. B. Mitchell, *Cancer Res.* **1987**, *47*, 936.
[67] N. G. Oliveira, M. Castro, A. S. Rodrigues, I. C. Goncalves, C. Martins, J. M. T. Rico, J. Rueff, *Mutat. Res. Genet. Toxicol. Environ. Mutagen.* **2005**, *583*, 36.
[68] M. Fenech, *Mutat. Res. Fundam. Mol. Mech. Mutagen.* **2000**, *455*, 81.
[69] P. Van Hummelen, M. Kirschvolders, *Mutagenesis* **1990**, *5*, 203.

Received: October 26, 2011
Published online: February 3, 2012

